University of South-Eastern Norway

Faculty of Technology, Natural Sciences and Maritime Sciences

–Master's Thesis

Study programme: Master of Science in Micro and Nano Systems Technology

Autumn 2023

Md Mehedi Billah

Feasibility of acoustically engineered backing material for ultrasound transducer.

Subtitle: additive manufacturing of tungsten loaded thermoplastic polyurethane (TPU)

University of South-Eastern Norway

Faculty of Technology, Natural Sciences and Maritime Sciences

Department of Microsystems.

Raveien 215

NO-3184 Borre, Norway

http://www.usn.no

Summary

The present study aims to examine the acoustic characteristics of a metamaterial made from tungsten loaded thermoplastic polyurethane (TPU) using COMSOL simulations. The investigation encompasses the simulation of single spheres with varied sizes, consecutive spheres with a fixed displacement, and spheres with different radii. The findings suggest that alterations in the dimensions and arrangement of spheres have a notable impact on resonance frequencies and acoustic absorption bandwidth. The objective of this study is to attain a broader absorption bandwidth at a frequency of 55 kHz. The simulations conducted in this research illustrate the possibility of modifying the parameters of the sphere to fulfil this objective.

Moreover, the thesis investigates the implications of employing two spheres with different sizes within a singular simulation, thereby uncovering the possibility of generating wider peaks and enhanced bandwidth. The inquiry additionally explores the correlation between the spacing of two distinct spheres and the resultant bandwidth, thereby offering valuable insights into the phenomenon of coupling.

In summary, this study makes a scholarly contribution to the advancement of optimum backing materials for underwater acoustic transducers. It provides an investigation into the impact of geometric parameters on acoustic behaviour. The results indicate that there are viable methods for customizing metamaterials to target specific frequency ranges, which could have potential uses in areas such as underwater exploration, navigation, and sonar systems.

Preface

I am pleased to present this thesis as a significant milestone in my journey through the master's program in Micro and Nano System Technology at the University of South Eastern Norway. The completion of this thesis would not have been possible without the invaluable guidance and support of several individuals, and I would like to express my deep appreciation for their contributions.

First and foremost, I would like to extend my gratitude to Professor Lars Hoff, my main supervisor, whose unwavering support, and mentorship have been instrumental in ensuring the successful execution of this research project. Throughout the year, he has provided me with invaluable insights and guidance, and I am deeply indebted to him for his mentorship.

I am equally indebted to my co-supervisor, Mr. Christopher Grinde, the Head of Transducer Design and Manufacturing at Nortek A/S. His mentorship and ability to convey complex concepts with clarity have been invaluable to me. Mr. Grinde not only provided me with the opportunity to work on this project a year ago but also maintained faith in my capabilities throughout the process. Without his guidance, this achievement would not have been possible.

I also wish to express my gratitude to the Nortek group for providing me with this unique opportunity and allowing me to delve into a new and challenging area of research. Collaborating with this esteemed company has been a rewarding experience that has broadened my knowledge and skills.

Finally, I dedicate this thesis to my late father, who is now at rest. I believe that if he were here today, he would take great pride in my accomplishments. May Allah bless him with Jannat.

Thank you to everyone who has been a part of this journey and has contributed to the successful completion of this thesis.

<Borre/29.10.2023>

<Md Mehedi Billah>.

Contents

Abbreviations

TPU: Thermoplastic Polyurethane

1 Introduction

An underwater acoustic transducer is a device that can convert the electrical signal to underwater acoustic waves and vice versa. It plays a vital role in a broad range of applications, such as ocean sampling networks, underwater exploration, navigation, sonar systems, distributed tactical surveillance, etc. [1]. This thesis is motivated to enhance the performance of low-frequency underwater acoustic transducers. There are several ways to improve the performance of underwater acoustic transducers. One way is by optimizing the backing material, which plays a big role in controlling its resonance frequency, bandwidth, and efficiency by damping unwanted vibrations and reflections. We aim to explore the effects of the metamaterials in backing using various design principles that are finely tuned to specific frequency ranges.

1.1 Motivation

The design of underwater transducers is significantly influenced by the broad range of frequencies that they may encounter in diverse applications. In order to enhance the performance of transducers across various frequency ranges, engineers are required to meticulously choose materials, geometry, and configurations that align with the particular demands of their intended application. This ensures that the transducer functions optimally with high efficiency within its designated frequency spectrum. In a broader context, underwater acoustic systems have traditionally covered a wide frequency range. The practical spectrum of underwater sound spans from approximately 1 Hz to well over 1 MHz, with the majority of applications occurring in expansive water bodies [2]. The research presented in this thesis involved collaboration with Nortek, a company specializing in the development of products for monitoring underwater movements through ultrasound technology, spanning frequencies ranging from 55 kHz to 6 MHz. There is the potential to utilize 3D printing techniques to produce structures with proportions suitable for the efficient manufacturing of designed metamaterials. Engineered acoustic metamaterials have the potential to facilitate the development of backing materials for underwater acoustic transducers that exhibit performance characteristics particular to both frequency and dissipation levels. For instance, the objective is to explore the feasibility of making such a material with consistent dissipation properties across a specified range of frequencies.

The research conducted in this thesis investigates whether a tungsten loaded scaffold embedded in matrix material can be used to engineer a dissipating backing structure. This scaffold is designed to possess a crystal-like structure, incorporating spherical resonators. For the lower range of frequencies indicated above, it may be possible to manufacture such scaffolds through additive manufacturing, opening the possibility for engineered materials with application-specific properties.

The work is to explore the engineered backing for a given frequency range. This means being able to design the amount of dampening rather than just maximizing it. Broader bandwidth engineering can give us a chance to choose a wide range of frequencies to transmit and receive acoustic signals. Our target is to achieve a broader bandwidth at a specific frequency of 55 kHz by changing the geometry. We could have chosen different target frequencies, such as 55 kHz, 100 kHz, 250 kHz, 333 kHz, 500 kHz, 1 MHz, etc. But the reason behind choosing 55 kHz is for the sake of simplicity; the wavelength becomes longer, and with the relevant dimensions, it is more likely that the additive structures we are exploring are feasible to manufacture.

1.2 Background of Acoustic Metamaterials

Acoustic metamaterials represent a category of artificially designed materials with unique properties for manipulating acoustic wave fields, characteristics that are not naturally present in conventional materials. The term "meta" has its origins in the Greek language, specifically derived from a word that denotes ‘beyond’ the properties or changes the properties of naturally occurring materials that are used to control acoustic wave propagation in exceptional ways [3]. There has been a notable emphasis on metamaterials in recent decades owing to their unique characteristics and the rapidly increasing ability to fabricate them [4]. The reason for the increased focus is that advances in manufacturing have made it easier to produce structures of relevant dimensions for metamaterials. The technological breakthroughs and special properties of metamaterials play a crucial role in the ever-growing field of metamaterial research, making them an interesting subject for investigation in this thesis.

Ma et al. [5] have introduced a locally resonant acoustic metamaterial, as depicted in (Figure 1). The presenter displayed a cross-sectional representation of a representative unit cell,

which comprised a tiny metallic sphere enveloped by a uniformly thin coating of silicone rubber. The illustration was situated on the left side of Figure 1. On the right side of Figure 1, the presenter showcased a sample that had been constructed by employing epoxy adhesive to bond together the unit cells shown on the left.

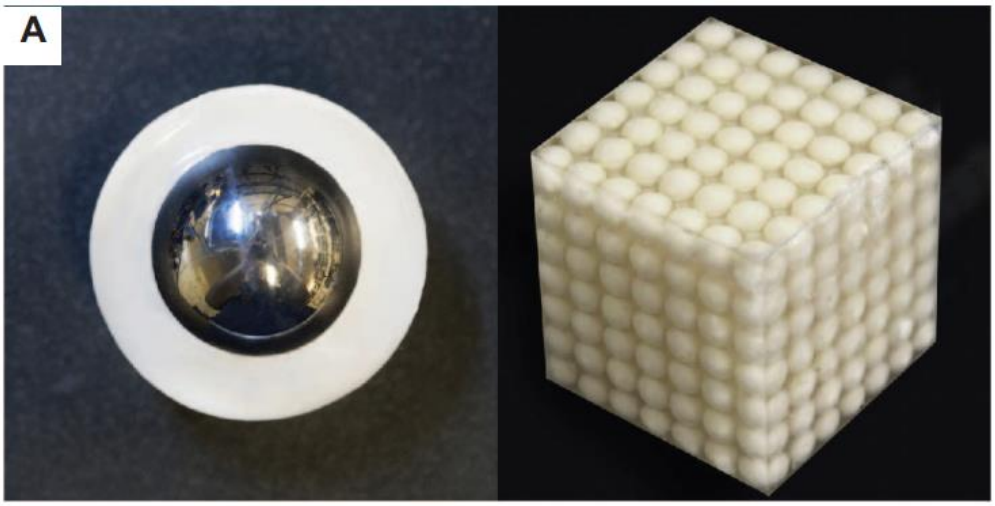

Figure 1 Initial realizations of locally resonant acoustic metamaterials [5].

1.2.1 Acoustic Metamaterial Characteristics for Sound Control

After the year 2000, metamaterials rapidly developed, and many new metamaterials emerged with numerous distinctive features, including negative bulk modulus, negative mass density, negative refraction, and subwavelength structure [4]. The important material characteristics of acoustic metamaterials include the effective mass density (ρ) and the effective bulk modulus (K). These properties can manipulate the acoustic wave's speed. Mike Haberman et al.'s [3] research highlights the fascinating capability of acoustic metamaterials to manipulate sound wave speeds, achieving extremes from exceedingly high velocities to near-zero or even negative speeds. This phenomenon arises from unconventional characteristics in both bulk modulus and mass density, where negative values of these properties contribute to unique and counterintuitive effects. Understanding this interplay offers new avenues for unprecedented control and modulation of acoustic wave behavior. Materials that possess either negative mass density and positive bulk modulus or positive mass density and negative bulk modulus are commonly referred to as single negative materials. Materials that possess a single-negative property do not support propagating waves. Consequently, any acoustic wave

present within such materials will undergo exponential decay. This characteristic makes them special and superior as sound absorbers.

1.3 Different Additive Manufacturing Techniques of Metamaterial

In the realm of manufacturing metamaterials, numerous additive manufacturing techniques are available, each characterized by distinct advantages and disadvantages. This section provides an overview of some of the most popular and widely utilized additive manufacturing methods for metamaterials.

Meisam et al. [6] extensively explored various additive manufacturing techniques in their study titled 'Additive Manufacturing of Metamaterials: A Review.' The research delves into different types of metamaterials and elucidates their manufacturing processes utilizing diverse additive manufacturing techniques.

The choice of a suitable additive manufacturing technique is of utmost importance in our research for creating a tungsten loaded thermoplastic polyurethane (TPU) metamaterial. The upcoming 'Discussion' section will provide a comprehensive assessment of how these methods correspond to our specific goals, taking into account the distinct needs and factors involved in achieving the desired metamaterial features in tungsten loaded TPU.

Stereolithography (SLA):

Stereolithography (SLA) stands out as a prominent additive manufacturing methodology, employing a liquid resin as its primary material. The curing process involves the sequential application of a precise laser or ultraviolet (UV) light, leading to the gradual solidification of the material layer by layer. This layer-by-layer solidification results in the formation of a sophisticated three-dimensional structure.

Selective Laser Sintering (SLS):

Selective Laser Sintering (SLS) is a popular 3D printing technology due to its numerous advantages and it represents a manufacturing process that selectively fuses powdered materials, including polymers or metals or ceramics, using a laser. The laser executes a layer-

by-layer sintering process to craft the final three-dimensional entity, showcasing the versatility of this technique.

Fused Deposition Modelling (FDM):

Fused Deposition Modelling (FDM) emerges as a widely employed additive manufacturing method. It entails the extrusion of thermoplastic filaments through a heated nozzle, depositing material in a layer-by-layer fashion to construct the intended configuration. FDM's prevalence lies in its accessibility and applicability for constructing structures with a variety of thermoplastic materials.

Electron Beam Melting (EBM):

Electron Beam Melting (EBM) stands as a widely adopted method in additive manufacturing, specifically leveraging metal materials. This technique utilizes an electron beam to selectively induce the melting and fusion of metal powders in a layer-by-layer manner, resulting in the creation of fully dense metal parts.

Inkjet 3D Printing:

Inkjet 3D Printing is characterized by the layer-by-layer deposition of liquid droplets onto a substrate. The subsequent solidification of these droplets culminates in the creation of the final three-dimensional configuration. This method showcases versatility in handling diverse materials, offering a unique approach to additive manufacturing.

While numerous other additive manufacturing techniques exist, Stereolithography, Selective Laser Sintering, Fused Deposition Modelling, Electron Beam Melting, and Inkjet 3D Printing represent the most common approaches in the field. In the discussion part, we will further explore the advantages and disadvantages of these techniques, providing valuable insights for determining the most suitable approach in the context of our metamaterial manufacturing.

1.4 Research Objectives

The mismatch of acoustic impedance between the piezoelectric material and water (the matching layer) can produce a ringing effect for pulse-echo applications, which is undesirable because it expands the pulse duration and lowers the bandwidth. To overcome this issue, a high impedance and absorptive backing material is used, which can dampen this ringing effect and increase the bandwidth. Typically, it's important to note that while matching layers are commonly used, in some cases, a backing material with a similar acoustic impedance to the transducer can be a preferred choice as it minimizes impedance mismatch and promotes efficient energy transfer within the system. However, it must be acknowledged that suppression of ringing or shortening of pulse duration is achieved by sacrificing sensitivity because a significant amount of energy is absorbed by the backing material. Several types of backing materials have been used, such as tungsten loaded epoxy, brass (70% Cu, 30% Zn), carbon, air, and different kinds of metamaterial [7]. Rojas et al. [8] have used a metamaterial made of 30% Al2O3 + EPO-TEK 301 epoxy as backing material for a 92-element phased array ultrasound transducer for cardiac imaging with X-ray computed tomography compatibility.

The primary objective of this research is to produce a specialized form of metamaterial using tungsten loaded TPU scaffolds to optimize the design by tailoring the dimensions of tungsten loaded TPU nodes in an Epotek 301-2 matrix to achieve a specific frequency and the spacing between said nodes. This study will further describe how two distinct spheres can effectively create a bandwidth between two dissimilar resonant frequencies and relevant prior research using COMSOL Multiphysics simulations and also discuss the additive manufacturing technique of tungsten loaded TPU.

1.5 Overview of Thesis Structure

The first chapter provides readers with an introduction to the underlying motivation behind the research and outlines the research objectives. Specifically, it clarifies the proposed approach for optimizing the backing of an underwater acoustic transducer at a specified frequency of 55 kHz. The chapter also talks about the history of acoustic metamaterials and why tungsten loaded TPU was chosen as the material of choice.

Chapter 2 will provide an overview of the theoretical framework underlying this research. It will encompass crucial definitions, including the theory of acoustic wave propagation, and explain the significance of these concepts. Additionally, the rationale behind selecting TPU as a material and its combination with tungsten will be expounded upon.

Chapter 3 will give an in-depth explanation of the technique employed, focusing primarily on the successive steps involved in conducting a finite element analysis of different sizes of tungsten loaded TPU and the spacing between them. Additionally, a detailed exposition will be presented on the systematic approach adopted for configuring the COMSOL model. Furthermore, a concise overview will be presented with the material properties of particular interest, namely tungsten loaded TPU and epoxy Epotek 301-2.

Chapter 4 is dedicated to the presentation of results. It begins with an exploration of the acoustic behaviour of metamaterials. Following this, we delve into a comprehensive analysis of simulation results involving varying sphere radii in tungsten loaded TPU and the spacing between pairs of spheres.

In Chapter 5, we will engage in the discussion phase, where we will expound on how the introduction of two distinct spheres can effectively establish a bandwidth spanning two different resonant frequencies. Additionally, we will scrutinize the impact of the spacing between these spheres on the resulting bandwidth. The discussion will also encompass the correlation between theory and expected results, potential weaknesses, and uncertainties inherent in our proposed model, any unexpected findings, and the connection between our approach and current studies in the field.

In the upcoming chapters, with particular emphasis on Chapter 6, we will provide a comprehensive presentation of the conclusive findings derived from the current study. Additionally, Chapter 7 will contribute valuable insights and propose potential avenues for future research endeavours within the scope of this subject matter.

2 Theoretical Background

2.1 Conventional Piezoelectric Transducer

The conventional piezoelectric transducer (Figure 2) is an electroacoustic transducer that converts mechanical energy into electrical energy and vice versa [7]. It incorporates a piezoelectric layer positioned between two active electrodes, supplemented by the addition of two additional layers. An additional layer, known as acoustic impedance matching, has been placed above the transducer to enhance the efficiency of energy transfer between the piezoelectric layer and the medium [7]. To mitigate reverberation and provide mechanical support to the active element, an additional layer known as backing has been added [9].

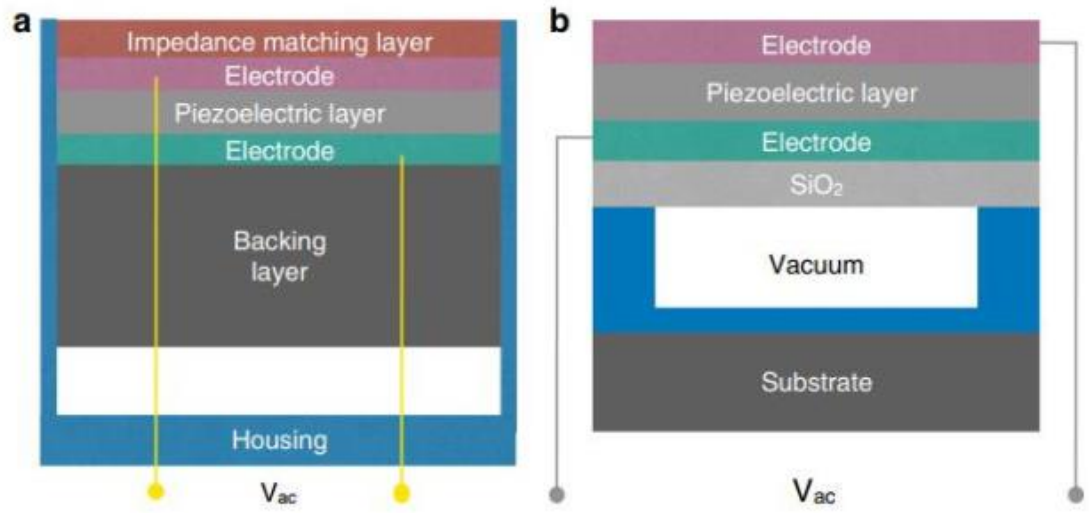

Figure 2 A Conventional Piezoelectric transducer.

2.2 Acoustic Wave Propagation Theory

Acoustic wave propagation theory is primarily concerned with understanding how sound behaves and travels through different materials and environments. Understanding the behavior of sounds is a fundamental theory that holds significant importance in the field of engineering. The behavior of sound in matter can be described by (Equation 1) known as the acoustic wave equation for sound pressure in one dimension, as follows:

$$\frac{\partial^2 X}{\partial x^2} = \frac{1}{v^2}\frac{\partial^2 X}{\partial t^2} \qquad (1)$$

The constant "v" denotes the velocity of sound and X is the displacement which varies with the change of position x and time t [10].

In the following discussion, we will explore the methodologies employed in determining the speed of sound as it traverses various media, including solids and liquids. The speed of sound in a solid is dependent on Young's modulus 'Y' and the density ‘ρ’ of the material can be expressed by (Equation 2) [11].

$$v = \sqrt{\frac{Y}{\rho}} \qquad (2)$$

We will now proceed to analyze the concepts of compressive wave speed and shear wave speed. In contrast to compressive waves as P-waves, which propagate through solid, liquid, and gaseous substances, shear waves, denoted as S-waves, often move at half of the P-wave speed in solids and do not propagate through liquids and gases [12]. The shear speed of sound can be calculated by given (Equation 3):

$$v_s = \sqrt{\frac{G}{\rho}} \qquad (3)$$

Where G represents the shear modulus or rigidity. The representation of the compressive wave speed is given by Equation 4 [13].

$$v_p = \sqrt{\frac{B+\frac{4}{3}G}{\rho}} \qquad (4)$$

The symbol "B" is used to represent the bulk modulus. The bulk modulus of a substance dictates its resistance to compression and serves as a measure of its incompressibility. As the bulk modulus of a material increases, its compressibility decreases. Considering the absence of S-waves in liquids meaning G=0, the speed of sound in a liquid can be determined using (Equation 5).

$$v = \sqrt{\frac{B}{\rho}} \qquad (5)$$

If one wishes to establish the relationship between Young's modulus and bulk modulus, it can be expressed using (Equation 6) [12]:

$$B = \frac{Y}{3(1-2n)} \quad (6)$$

Where ‘B’ is the Bulk modulus, ‘Y’ represents Young’s modulus and ‘n’ denotes the Poisson’s ratio.

2.2.1 Sound Absorption by Propagation

The transmission of a sound wave is linked to the transfer of acoustic energy. The energy can be separated into two distinct forms: kinetic energy and potential energy. A phenomenon observed during the propagation of acoustic waves is the decrease in intensity, mostly attributed to the geometric dispersion and absorption of acoustic energy by the medium through which the waves propagate. The measurement of propagation loss holds significant importance in acoustic systems, as it serves to limit the loudness of the received signal [14].

Attenuation is a crucial factor in limiting the loudness of a received signal. When sound waves encounter obstacles or pass through materials, a portion of the sound energy is either absorbed or scattered within the medium, resulting in a reduction in signal volume. Propagation loss measurement is crucial for researchers and engineers, providing essential insights into signal loss in specific mediums. This understanding informs informed decision-making for optimizing transducers and acoustic systems by fine-tuning parameters like power and signal processing for improved signal volume and quality.

2.2.2 Quarter Wavelength Resonance and Its Impact on Sound Absorption

A quarter wave resonator (Figure 3) that is open on one side and closed on the other, with a length equal to one-fourth of the wavelength of the sound wave it contains is referred to as a quarter wavelength resonator [15].

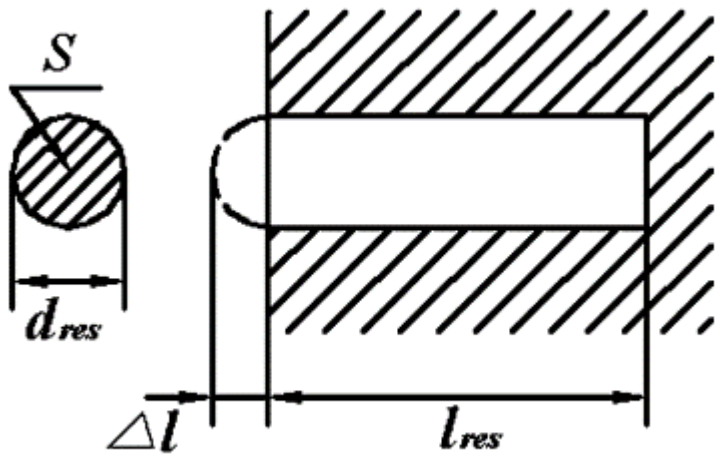

Figure 3 Quarter Wavelength Resonator [16].

The quarter-wavelength resonator is a fundamental component frequently employed in acoustics. Resonance occurs when an odd multiple of a quarter of the wavelength matches the resonator's radius. At these resonant frequencies, maximum sound absorption occurs, primarily due to the effect of elastic dissipation. The magnitude of these effects is chiefly dictated by the resonator's radius, as it plays a critical role in determining the primary frequencies at which sound is absorbed.

Quarter-wavelength resonators are often utilized for attenuating acoustic waves, both for insulation and dissipation purposes, and also utilized as an impedance transformer. This thesis focuses on the realm of acoustic dissipation. At the resonant frequency, notable gradients in velocity and temperature arise within the boundary layer, leading to varying degrees of energy dissipation from the incident wave. Especially, at the resonance frequency, dissipation reaches its peak due to the dominant influence of internal frictional forces, which transform the wave's energy into heat through the Joule effect [15].

The resonant frequency, denoted as fres, can be mathematically expressed by (Equation 7) [17].

$$\text{fres} = \frac{(2m-1)V_0}{4l_{res}} \qquad (7)$$

Where V_0 is the speed of sound, f is the frequency and m is an integer, and *l*res denotes the length of a quarter wavelength resonator.

In perfect absorption, the reflected wave from one side exhibits a phase shift of 180 degrees, resulting in destructive interference, especially for hard materials [18]. This phenomenon offers a straightforward approach to achieving optimal sound absorption by wave cancellation. Destructive interference (Figure 4), also known as 180-degree, out-of-phase interference, arises when the crests of one wave coincide with the troughs of another wave, leading to the cancellation of positive and negative amplitudes, resulting in a wave with no amplitude [18].

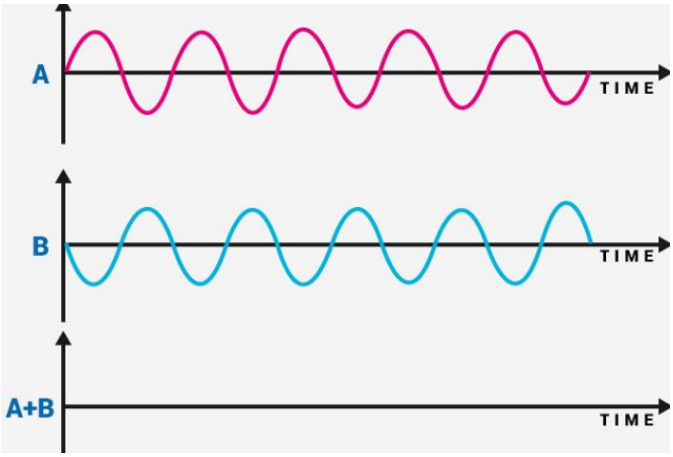

Figure 4 Presentation of a destructive interference [18].

2.3 Mechanics of Tungsten Loaded TPU in Epoxy Matrices

There are various methods to explore the backing material, such as modifying its composition, altering its thickness, or changing its structural properties. In this research, we will explore the advancement of backing materials for low-frequency underwater acoustic transducers. We will utilize tungsten loaded TPU scaffolds to absorb energy in terms of undesired vibrations and reflections within the backing. By changing the geometry of the spheres of tungsten loaded TPU, we will be able to fix the specific frequency range. The present study involves the experimental synthesis of an artificially designed material, commonly referred to as a metamaterial, by combining TPU and tungsten in various trials. The following part will explain the motivation and objective of the amalgamation and selection of these two items.

2.4 A Material for Sound Attenuation and Vibration Damping

Rubber is widely recognized for its versatility as an elastomeric material, and its unique viscoelastic qualities and frequency-dependent damping characteristics contribute significantly to its role in sound attenuation. The efficacy of rubber in sound mitigation is derived from its distinctive capacity to convert kinetic energy into thermal energy, resulting in the efficient dissipation of sound energy [19].

One interesting characteristic of rubber is its ability to undergo significant elastic deformation when subjected to vibrations and sound waves, promptly returning to its original shape afterward. The behavior plays a critical role in the reduction of noise and vibration, as rubber demonstrates a noticeable delay in its deformation concerning variations in stress [20] [21]. The energy conversion process included in rubber serves the dual purpose of attenuating sound and reducing sound reverberation inside a confined area. [19] Moreover, the adaptability of rubber extends beyond its inherent qualities. Rubber, when appropriately blended with other compounds, demonstrates improved damping properties, rendering it a valuable component in composite materials engineered for mitigating noise and vibration [21].

In summary, rubber is considered a preferred material for achieving comprehensive noise and vibration reduction due to its viscoelastic properties, frequency-dependent damping, and enhanced damping characteristics resulting from blending with other compounds, along with distinctive energy conversion skills, is deemed a preferred material in the endeavor to achieve comprehensive noise and vibration reduction.

2.5 Properties and Behaviour of Tungsten in Acoustic Materials

Tungsten, known for its high density and acoustic velocity. Incorporating tungsten particles into epoxy resin has been demonstrated to significantly improve dissipation compared to epoxy resin without tungsten particles. This enhancement is attributed to various factors, including differences in density, acoustic impedance matching, as well as scattering and absorption phenomena. Due to its high density, the addition of tungsten into epoxy results in an increase in the overall density of the composite. Consequently, the enhanced density

facilitates a significant interaction between sound waves and the constituent materials, leading to higher energy losses through scattering and absorption. [22]

2.6 Key Variables in Proposed Metamaterial Design

The research will encompass a thorough examination of various crucial aspects pertaining to the design of frequency-specific acoustic metamaterials. Key variables to be investigated include:

Material Setup and Frequency Range Simulation: This involves simulating a single frequency to determine the speed of sound.

Sweeping Single Sphere Radius: The radius of a single sphere of tungsten loaded TPU will be systematically varied to identify the specific resonance frequency for a particular sphere.

Sweeping Two Consecutive Spheres: This step entails sweeping the radius of two consecutive spheres of tungsten loaded TPU to compare the resonance frequency behavior with the simulation involving a single sphere.

Sweeping Spacing Between Two Spheres: The investigation will involve varying the spacing between two consecutive tungsten loaded TPU spheres to observe its impact on resonance frequency.

Combining Multiple Sphere Sizes and Spacing: Finally, different sphere sizes will be combined, and various spacings between spheres will be explored to achieve desirable "bandwidth enhancement" characteristics.

These steps will be comprehensively explained in the subsequent Method section, with a detailed discussion of their implications on the results presented in the Results section.

3 Methods

In this section, we will engage in a description of tungsten loaded TPU composites and the material characterization techniques and an in-depth analysis of the COMSOL simulation process, systematically explaining each stage and entering the exploration of various simulation methodologies.

3.1 An Overview of TPU-Epoxy-Tungsten Composites

This section will focus on the examination of TPU epoxy tungsten composites, specifically the combination of 10% tungsten with 90% TPU, as well as the advantages derived from the amalgamation of these two substances. The incorporation of tungsten into TPU composites leads to a significant increase in the composite's total mass owing to the high density of tungsten. This augmented mass, in turn, contributes to enhanced damping characteristics by providing more resistance to motion, providing a notable benefit to the composite material. A material with higher density has an enhanced capacity for energy absorption, as it effectively dissipates sound energy by transforming it into heat energy through internal friction and vibrations. Moreover, the increase in mass can reduce the resonance frequency due to the greater resistance to changes in motion exhibited by a larger mass. This results in a slower oscillation, and concurrently, it amplifies the damping effect across a broad range of frequencies. The interaction can be further described through (Equation 8), which demonstrates how the slowed oscillation enhances the overall damping response. Finally, the utilization of impedance matching with the surrounding material can facilitate the improvement of acoustic energy transfer by minimizing reflections. This enables a more efficient transmission of sound energy from the transducer to the medium. In addition to these numerous advantages, our primary motivation for developing TPU-epoxy-tungsten composites stems from the unique properties of TPU, especially its softness and its ease of 3D printing when combined with tungsten. The general solution for the response of an overdamped harmonic oscillator can be expressed as [23]:

$$x(t) = e^{-\beta t}\left[A_1\, cos(\omega_2 t) + A_2\, cos(-\omega_2 t)\right] \qquad (8)$$

Where, x(t) is the displacement at time t, A1 and A2 are the amplitude, β is the damping parameter, ω_2 is the damped angular frequency.

This relation between a slower oscillation (larger β) and an amplified damping effect suggests that an increased damping parameter results in a more expedited dissipation of oscillation over time.

3.2 Material Characterization Techniques

In our study, we focus on TPU as our primary material, supplied by Nortek. The selection of TPU from Nortek was influenced by the availability of samples as we had already initiated this work. Our commitment to research reliability and consistency prompted us to use the TPU samples that were readily accessible. It's essential to note that traditional TPUs may exhibit varying material properties in different conditions, which further reinforced our decision to utilize the available TPU from Nortek for the sake of research consistency.

Initially, we calculated the density of the TPU sample and determined the speed of sound. We then assessed the impact of introducing tungsten, analyzing the resulting speed of sound, and simulating potential benefits. In the following sections, we will briefly outline our method for TPU density calculation, setting the stage for exploring its acoustic properties.

The calculation of the speed of sound has been performed by employing slide calipers and a weighing scale (Figure 5). This apparatus has been used to determine the density of the sample. Slide calipers were employed to measure the radius and thickness of the sample, while a weighing scale was used to measure its mass.

Figure 5 Identification of thickness, radius, and mass using slide calipers and a weighing scale.

The density of our sample has been determined using the utilization of (Equation 9).

$$\rho = \frac{M}{A \cdot t} \qquad (9)$$

Where A represents the area of the disc, t denotes the thickness of the disc, and M symbolizes the mass of the disc.

$$A = \pi r^2 = 4.87 * 10\text{-}4\ m^2,$$

$$t = 4.3 * 10^{-3}\ m \text{ and } M = 2.11 * 10^{-3}\ kg.$$

Upon performing the necessary calculations for (Equation 9), it has been determined that the density of the TPU material is 1009 kgm^{-3}.

The composition of the material will consist of 10% tungsten and 90% TPU. The density of tungsten is around 19300 kgm-3 [24]. The resulting composite material consisting of tungsten loaded TPU will exhibit a total density.

$$\rho TLR = (0.1 * 19300 + 0.9 * 1009)\ Kgm^{-3} = 2837\ kgm^{-3} \qquad (10)$$

3.2.1 Investigation of Material Properties in Tungsten Loaded TPU

In his paper, D. Tabor found the bulk modulus of a typical TPU to be around 10^9 Pa [25]. This value, attributed to a typical TPU, serves as a reference for our TPU.

Given the absence of precise material properties for tungsten loaded TPU in our current dataset, we find it necessary to assume the bulk modulus value for tungsten loaded TPU. This assumption becomes an integral step in our analysis as we explore and characterize the acoustic properties of the composite material.

Given tungsten's renowned high density, we anticipated an increase in the material's bulk modulus (B_{TLR}) by incorporating it into TPU. To provide a theoretical basis for this assumption, we considered the Voigt-Reuss-Hill average [26][27], a model commonly used for estimating bulk modulus in composite materials. However, it's important to acknowledge the influence of material processing on the actual composite properties. Factors such as the distribution of tungsten particles, and bonding characteristics introduced during processing can impact the bulk modulus. While the theoretical estimate, accounting for various factors and using the VRH average, predicted an increase of approximately 3.5 x 10^9 Pa, the actual observed increase may vary due to the intricacies of material processing and real-world conditions.

The speed of sound through tungsten loaded TPU has been determined using (Equation 5) and a given value for the density of tungsten loaded TPU (ρ_{TLR}) from (Equation 10).

$$v_{TLR} = \sqrt{\frac{B_{TLR}}{\rho_{TLR}}} \tag{11}$$

The calculated speed of sound in tungsten loaded TPU has been calculated by (Equation 11) and is approximately 1111 m/s. The wavelength of tungsten loaded TPU indicated as λTLR, has been determined by utilizing the speed of sound from (Equation 11) at the target frequency of 55 kHz.

$$\lambda_{TLR} = \frac{v_{TLR}}{f_c} \tag{12}$$

Where, V_{TLR} denotes the speed of sound through tungsten loaded TPU and fc denotes 55 kHz.

3.2.2 Investigation of Material Properties in Epotek 301-2

The determination of the speed of sound in a material involves the utilization of acoustic impedance and density in the calculation process.

$$Z = \rho C \quad (13)$$

In the context of this study, Z signifies acoustic impedance, ρ represents density, and C denotes the speed of sound, the values of acoustic impedance and density for Epotek 301-2 are 3.05 x 10^6 Rayls and 1150 kgm^{-3} respectively (Table 2). Utilizing these values in (Equation 13), we ascertain that the speed of sound through Epotek 301-2 is approximately 2650 m/s.

The wavelength of Epotek 301-2 is subsequently determined by employing the speed of sound and the target frequency of 55 kHz in (Equation 14):

$$\lambda e = \frac{V_e}{f_c} \quad (14)$$

Where, V_e denotes the speed of sound through Epotek 301-2 and fc denotes 55 kHz.

3.2.3 Investigation of Material Properties of Tungsten Loaded TPU and Epotek 301-2 for COMSOL Simulation

In order to generate blank material in a COMSOL simulation, it is necessary to specify three material properties. Three fundamental material properties are commonly considered in the fields of materials science and engineering. These properties are density, Young's modulus, and Poisson's ratio. TPU has a consistently approximate Poisson's ratio of close to 0.5 and exhibits variations within the range of 0.4 to 0.499, whereas tungsten demonstrates a comparatively lower Poisson's ratio of approximately 0.27 [24]. Therefore, it has been assumed that the Poisson's ratio in tungsten loaded TPU is approximately 0.45. The Young's modulus of tungsten loaded TPU has been determined by reorganizing (Equation 15).

$$B = \frac{Y}{3(1-2n)} \quad (15)$$

In the given context, the symbols B, Y, and n represent the bulk modulus, Young's modulus, and Poisson's ratio, respectively. Upon calculating (Equation 3.8), it is determined that Young's modulus of tungsten loaded TPU is around 1.04 GPa. Through these analyses, we have successfully identified all the material parameters associated with tungsten loaded TPU.

In order to simulate the Epotek 301-2 in COMSOL, the material parameters, including Young's Modulus, Density, and Poisson's ratio, have been sourced from (Table 2)

3.3 Description of COMSOL Simulation Setup and Parameters

3.3.1 Study and Properties:

The present model is based on a two-dimensional spatial dimension framework, wherein the solid mechanics part has been chosen from the Physics section with frequency domain from COMSOL. The simulation of the model at a certain frequency of 55 kHz has been chosen to investigate the velocity of sound propagation through the materials. This decision was made after configuring the geometry, materials, solid mechanics, and mesh components. Following the simulation (Section 4.1), the speed of sound through tungsten loaded TPU was determined to be 1178 m/s, while for Epotek 301-2, it was found to be 2471 m/s. Additionally, the wavelength of sound waves at a specified frequency (55 kHz) was calculated for both materials, resulting in wavelengths of 44.927 mm for Epotek 301-2 and 21.418 mm for tungsten loaded TPU. In (Table 1), the expression "epo301-2. lambda" denotes the wavelength of Epotek 301-2, while "TLR.lambda" represents the wavelength of tungsten loaded TPU. The parameters for COMSOL simulation will be specified in (Table 1), provided below:

Table 1 Chosen Parameters for COMSOL Simulation

Name	Symbol	Expression	Value
Thickness of the whole model	H	1.8*epo301-2.lambda	80.869 mm
Width of the model	w	1.8*epo301-2.lambda	80.869 mm
Speed of sound in Epotek 301-2	V_e	epo301.c	2471 m/s
Speed of sound in tungsten loaded TPU	V_{TLR}	TLR.c	1178 m/s
Center frequency	F_0	-	55 kHz
Wavelength of Epotek 301-2	λ_e	epo301-2. lambda	44.927 mm
Wavelength of tungsten loaded TPU	λ_{TLR}	TLR.lambda	21.418 mm
Radius of sphere	R	-	5.35 mm
Distance between two spheres	D	-	11.232 mm
Minimum frequency	f_{min}	-	30 kHz
Frequency step	f_{step}	-	0.125 kHz
Maximum frequency	f_{max}	-	80 kHz

3.3.2 Geometry:

The simulation system consists of three independent domains (Figure 6). Every domain has a significant role to play in the attainment of precise and enlightening outcomes. To improve clarity and comprehension, descriptive labels have been allocated to each domain.

Backing Core (Domain 1): Domain 1 signifies the fundamental essence of the support. The epoxy material, Epotek 301-2, is enclosed within a square zone to effectively absorb the energy applied from the top of the square as a boundary load.

Perfectly Matched Layer (Domain 2): Domain 2 encompasses a region with a thickness of 8mm, wherein the implementation of the perfectly matched layer (PML) is situated within that square zone. The presence of the Perfectly Matched Layer (PML) is crucial to effectively reduce reflection and enhance the absorption of acoustic energy. This, in turn, leads to a more accurate representation of wave interactions in simulations.

Tungsten loaded TPU Inclusion (Domain 3): The inclusion of Tungsten loaded TPU (Domain 3) is confined to a circular zone within the square shape of the backing. The aforementioned inclusion refers to the metamaterial employed to absorb the energy imparted by the top of the square as a boundary load.

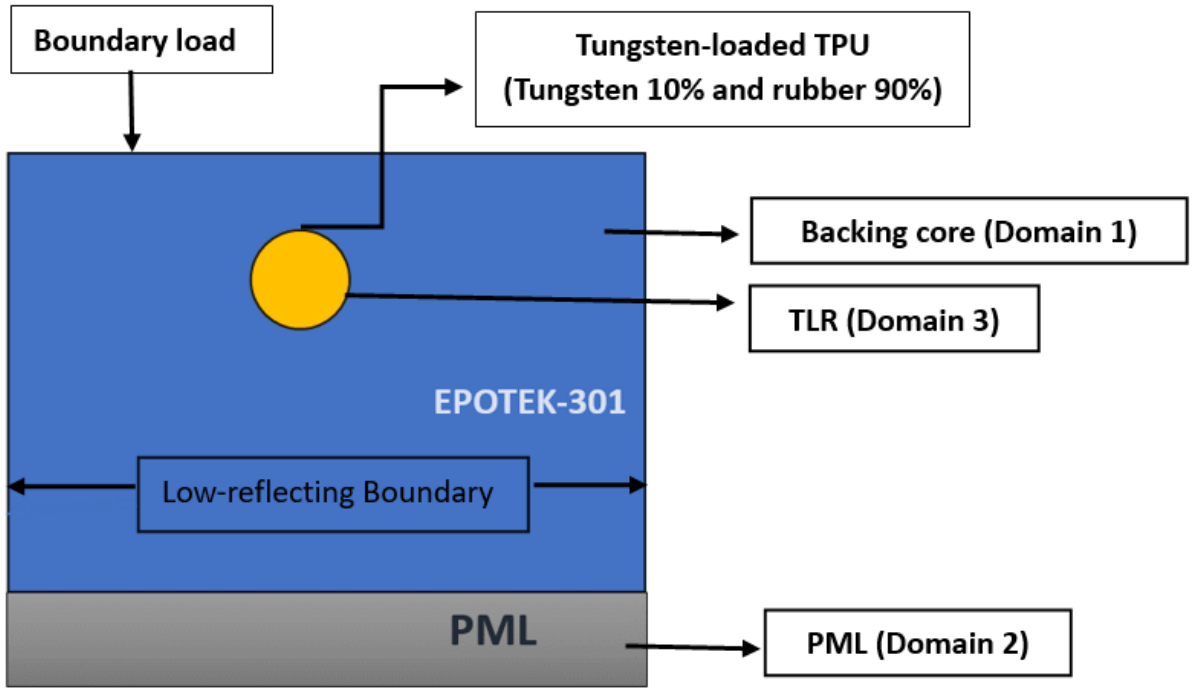

Figure 6 Geometry of COMSOL Simulation Model

3.3.3 Materials:

A material model for tungsten loaded TPU, which contains 10% tungsten and 90% TPU, has been defined by utilizing blank material from the material section in COMSOL Multiphysics. This material has been specifically chosen for implementation within the circular domain. Using the identical methodology, we made Epotek 301-2 (an epoxy material), which has been chosen for application in the backing core including a perfectly matched layer (PML) region. The properties of both materials are shown in the subsequent (Table 2).

Isotropic loss Factor:

In COMSOL, various damping types are available [28], including Rayleigh Damping, Isotropic Loss Factor, Anisotropic Loss Factor, Orthotropic Loss Factor, and Viscous Damping. Among these, for frequency domain analysis encompassing all material types, the Isotropic Loss Factor is deemed appropriate, aligning well with our investigation's focus on frequency domain analysis. Consequently, we have selected the Isotropic Loss Factor as the damping parameter.

Our primary objective is to effectively absorb a significant amount of energy in tungsten loaded TPU. Accordingly, we have designated the isotropic loss factor in Epotek 301-2 to be one-tenth of the isotropic loss factor of tungsten loaded TPU. This choice is made with the recognition that real-world scenarios involve some energy absorption in Epotek 301-2, acknowledging that complete energy absorption cannot be achieved solely through the tungsten loaded TPU sphere.

Table 2 Different Properties of Selected Materials

	Tungsten loaded TPU	Epotek 301-2 (epoxy)
Young's modulus	1.04 X 10^9 Pa	3.66 X 10^9 Pa[29]
Poisson ratio	0.45	0.358[29]
Bulk Modulus	3.5 X 10^9 Pa	4.3 X 10^9 Pa
Speed of Sound	1178 m/s	2471 m/s
Acoustic Impedance	-	3.05 X 10^6 Rayls[30]
Density	2837 kgm^{-3}	1150 kgm^{-3}[30]
Isotropic loss factor	0.1 [31]	0.01

A detailed explanation of the properties of Tungsten loaded TPU can be found in (Section 3.2.1).

3.3.4 Physics (Solid Mechanics):

In this section, two linear elastic material sections have been employed for both Epotek 301-2 and tungsten loaded TPU. Damping has been introduced by including isotropic loss factors with varying values (Table 2) for both Epotek 301-2 and tungsten loaded TPU.

3.3.4.1 Boundary Conditions:

The model is subject to two boundary conditions. The first is the boundary load, which exerts a force per unit area (5 Nm-2) on the top of the model.

The final boundary condition corresponds to the low reflecting boundary. The utilization of a low reflecting boundary on the lateral sides of the wall serves the objective of mitigating any excessive reflections from the walls within our model [32].

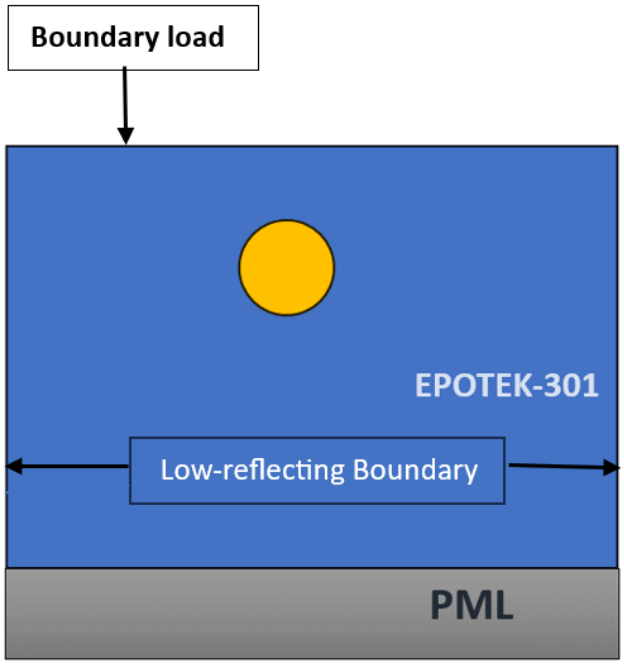

Figure 7 Boundary Conditions of the Model

3.3.5 Mesh of the Model:

In the COMSOL simulation, a free triangular mesh has been used for domains 1 and 3, while a mapped mesh has been selected for the perfectly matched layer section. The determination of the maximum element size for the mesh is guided by the consideration of the wavelength (one-fifth) across different materials. The choice of setting the maximum element size as one-fifth of the wavelength is crucial for ensuring model stability. The rationale for selecting a mesh element size that is equal to or smaller than one-fifth of the wavelength is rooted in the

Nyquist criterion. This criterion establishes a minimum need of two points per wavelength to get an accurate representation of the wave within the mesh [33].

This wavelength is typically calculated by identifying the highest frequency within the desired frequency range. In our investigation, we have established the maximum element size for domains 1 and 2 by performing calculations based on the wavelength of the Epotek 301-2 material. Likewise, for domain 3, we have applied the wavelength of tungsten loaded TPU material.

3.3.6 Frequency Domain and Parametric Sweep Analysis:

In conducting the frequency domain analysis, our model is simulated across a specific spectrum of frequencies. The chosen frequency range for this study encompasses 30 kHz to 80 kHz, wherein 30 kHz designates the minimum frequency (fmin) and 80 kHz represents the maximum frequency (fmax). The selection of this frequency range is strategically centered around our specified central frequency, which is set at 55 kHz. The determination of the center frequency is based on the average of the minimum and maximum frequencies, providing a balanced and representative focal point for our analysis. This approach ensures that our simulation captures a comprehensive view of the system's behavior across the chosen frequency spectrum.

In the field of product development, it is frequently important to address multiple iterations of a given model to determine the ideal features of its design. Instead of manually modifying these property values and resolving the problem repeatedly, an alternative approach is to conduct a parametric sweep using COMSOL Multiphysics. A parametric sweep enables the manipulation of parameter values within a specified range [34]. In this experiment, the parametric sweep technique is being used to calculate various sphere sizes and spacing configurations between spheres.

3.4 Exploration of Various Forms of Simulations

This section will provide a comprehensive account of the investigations conducted on different types of simulations, focusing on the methodical investigation of varying sphere sizes, and spacing between the spheres.

3.4.1 Material Setup and Single Frequency Simulations

This simulation aims to examine the velocity of sound propagation in two distinct materials, namely Epotek 301-2 and tungsten loaded TPU. Once the material parameters of both materials have been established, we proceed to mimic the frequency domain by applying a single frequency of 55 kHz. Upon determining the velocity of sound propagation in the substances, we have subsequently computed the wavelength of such substances by using (Equation 14) at a frequency of 55 kHz. The wavelengths of both materials have been utilized to establish the square and circular domains. The square domain has been established by employing a dimension that is 1.8 times the length of a quarter wavelength of λe.

3.4.2 Sweeping Sphere Radius

The circular part has been designed by using the wavelength passing through tungsten loaded TPU material at a frequency of 55 kHz. The quarter-wavelength of tungsten loaded TPU, which means $\lambda_{TLR}/4$ (Figure 8) has been utilized to create the sphere. After setting up this model, we have used parametric sweep for multiple simulations together by using the sphere radius from, e.g.,0.93 $\lambda_{TLR}/4$ to 1.14 $\lambda_{TLR}/4$ in steps of 0.07 $\lambda_{TLR}/4$. These steps will give us different resonant frequencies for each step. Further explanation will be discussed in the result section.

Note: The justification for selecting multiplication factors such as 0.93 or 1.14, in conjunction with the quarter wavelength of tungsten loaded TPU, while avoiding precise multiples of 0.25, lies in the desire to create a versatile model. This approach enables the exploration of gradual changes in the system's behavior, moving beyond a focus solely on peak values. By avoiding strict adherence to specific multiples, the model becomes flexible enough to capture various phenomena and offers a more detailed representation of the system's dynamics.

3.4.3 Sweeping Radius of Two Spheres Maintaining a Fixed Displacement

This section aims to elucidate the energy absorption capabilities of two tungsten loaded TPU spheres when positioned consecutively at a distance equivalent to one-quarter of the wavelength of Epotek 301-2 (λe/4), recognizing this spacing as a deliberate design parameter. The parameter λe/4, as depicted in (Figure 8), is not merely a geometric constraint but is strategically chosen to shape the material's response to external factors. We will modify the dimensions of the spheres according to the specifications outlined in Section 3.4.2. Specifically, we will adjust the size from 0.93 $\lambda_{TLR}/4$ to 1.14 $\lambda_{TLR}/4$ in steps of 0.07 $\lambda_{TLR}/4$ by ensuring a consistent spacing λe/4 between the two spheres. The obtained results will be compared to Section 3.4.2 in the result and discussion section.

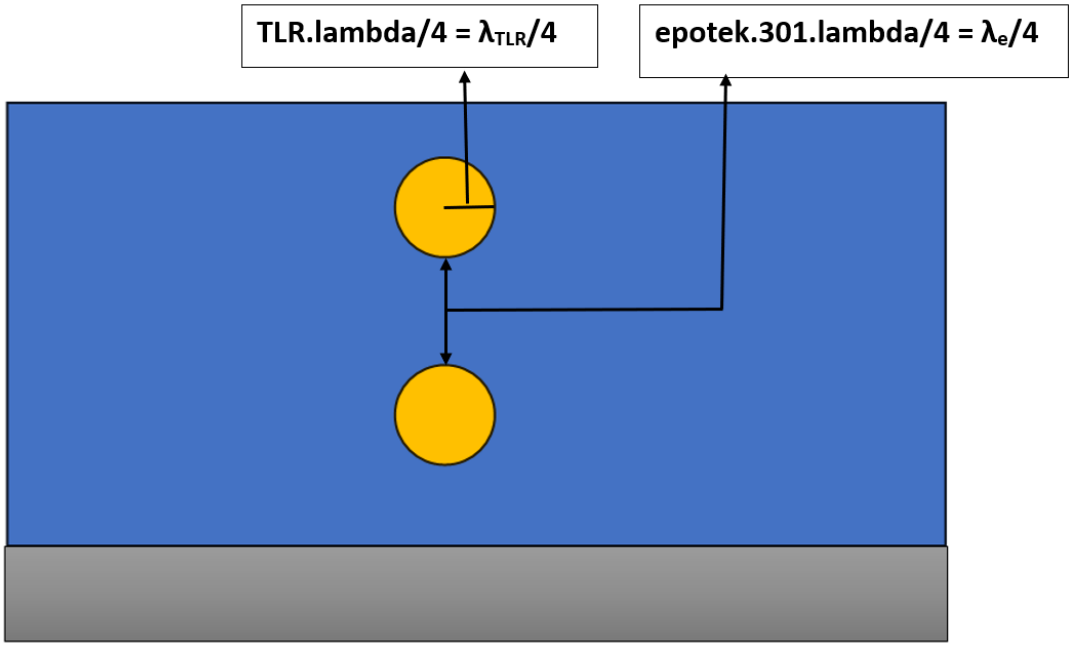

Figure 8 Two Tungsten-loaded TPU spheres maintaining a distance λe/4.

3.4.4 Sweeping Parametric Spacing

The model has been adjusted by maintaining a consistent gap of a quarter wavelength of Epotek 301-2 between two spheres. In this section, we are going to investigate how the space between two spheres influences absorbing energy.

The distance between the spheres will be varied incrementally, specifically, we will modify the spacing ranging from 1.43 λe/4 to 2.00 λe/4 with an increment of 0.19 λe/4. Throughout this investigation, the radius of the spheres ($\lambda_{TLR}/4$) will remain constant.

3.4.5 Simulation of Spheres with Different Radius

Upon conducting a comprehensive analysis and precise identification of all the simulations, it will become feasible to determine the specific sphere that is accountable for each resonance peak. Once the resonance peak of a certain sphere has been determined, it becomes possible to ascertain the flatness of the band by employing spheres with different radii (Figure 9) in a single simulation. This can be achieved by initially maintaining a consistent distance between the spheres and subsequently altering the spacing between them. Following the completion of this simulation, our objective is to establish the association between spheres with different radii and a specific band.

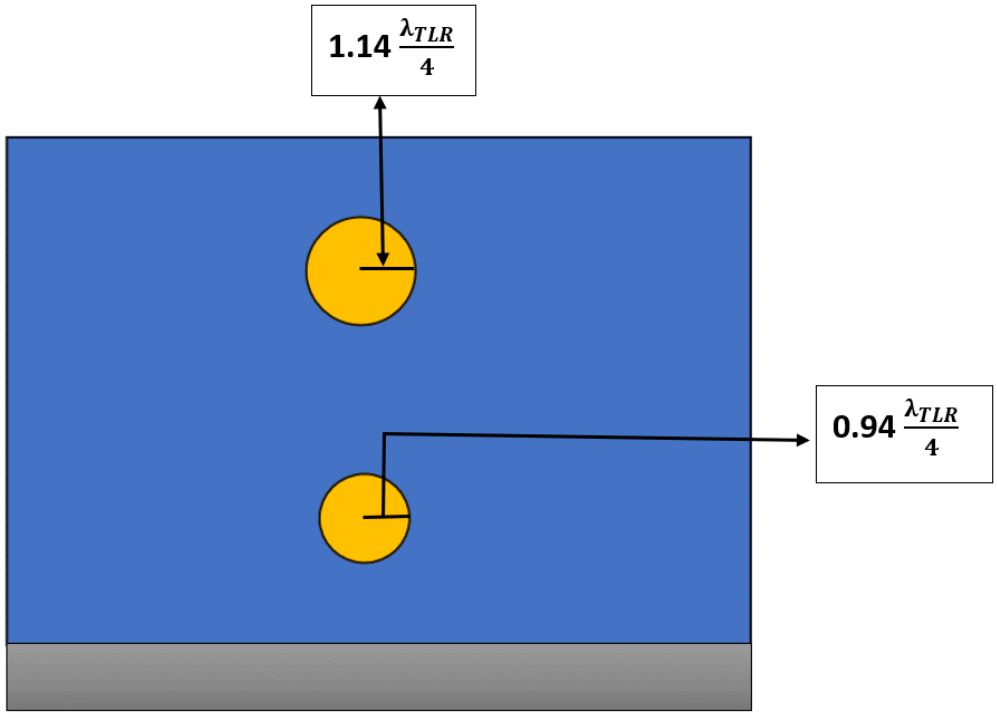

Figure 9 Using spheres with different radii for identifying a broader bandwidth.

4 Results

In this section, we will delve into the examination of the acoustic behavior within the metamaterial. Furthermore, we will scrutinize the outcomes of the various simulations outlined in the methodology section.

4.1 Simulation Result of Acoustic Behaviour in the Meta-Material

After setting all the material parameters (Section 3.3.3) and mesh elements (Section 3.3.5) in the COMSOL simulation, a single-frequency simulation was conducted at 55 kHz to determine the speed of sound.

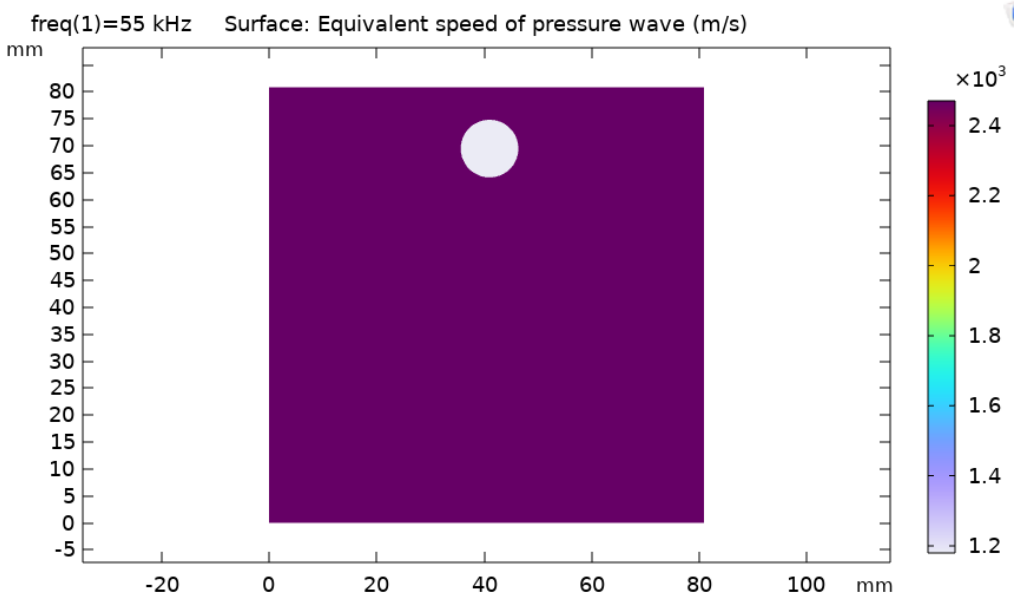

Figure 10 COMSOL simulation for identifying the speed of sound through different materials.

Upon doing the simulation, we determined the equivalent speed of the pressure wave (m/s) by referring to the expression section in the settings. After performing the simulation on the structure at a specific frequency at 55 kHz, it was established that the tungsten loaded TPU displayed a pressure wave speed of 1178 m/s. In contrast, Epotek 301-2 exhibited a pressure wave speed of 2471 m/s. The determination of sound speed across various materials involved utilizing material properties such as Young's modulus, Poisson's ratio, and density obtained

from (Table 1) for both tungsten loaded TPU and Epotek 301-2. The white circle depicted in (Figure 10) represents the tungsten loaded TPU. Conversely, the violet portion represents the epoxy Epotek 301-2.

4.2 Comparison of Simulation Result with Analytical Analysis

If we desire to compare the simulated speed of sound with the analytically estimated speed of sound for tungsten loaded TPU, it is evident that there is minimal disparity between these two figures. The speed of sound through the tungsten loaded TPU was determined analytically to be around 1111 m/s. However, the value obtained by the COMSOL simulation was found to be 1178 m/s. The discrepancy might be disregarded since we have assumed the poison's ratio and the bulk modulus of tungsten loaded TPU. Based on the obtained value of the speed of sound through tungsten loaded TPU from the COMSOL simulation, we will proceed with conducting further simulations.

For Epotek 301-2, a comparison between the analytical approach and simulated results reveals a slight discrepancy in the speed of sound. The analytical calculation yields a speed of around 2650 m/s, while the simulation indicates a value of approximately 2471 m/s. It is crucial to acknowledge the impact of several elements, including material heterogeneity, boundary conditions, and inherent assumptions, on the simulation model. Considering the complexities and limitations associated with simulations, we proceed with the results provided by COMSOL for our further analyses.

4.3 Model Stability Checking

Ensuring the changing of the dimensions of the backing core has no impact on our model is imperative. This is critical because any influence of dimension changes on our results would complicate the isolation of the primary effects on our design elements, specifically the tungsten loaded TPU. Therefore, an analysis is necessary to ascertain that alterations in model dimensions do not affect the energy loss spectrum. Our foremost goal is to accurately capture energy absorption within the tungsten loaded TPU and the epoxy material, Epotek301-2. Model dimensions maintain uniformity, as depicted in (Figure 11), where both width (w) and height (H) are set at 1.8 times the value of Epotek 301-2. lambda.

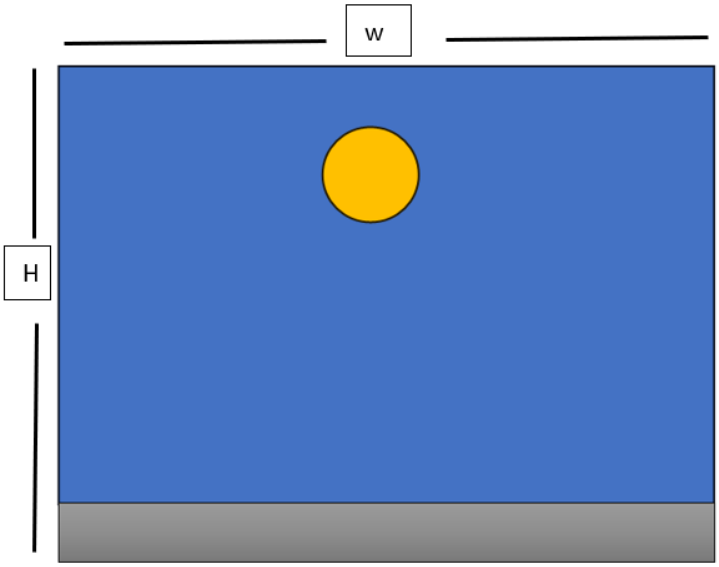

Figure 11 Width and height measurement of the model

In this study, we sought to investigate the relationship between varying model heights and the loss vs. frequency spectrum. This objective was to notice any potential alterations in the spectrum resulting from these changes. If any alterations are observed in the spectrum, it would indicate that the dimension has a significant influence on the result, necessitating its removal. Our study employed three distinct height values: 1.8 times that of $\lambda e = 22.464$ mm, 2.3 times of $\lambda e = 44.927$ mm, and 2.8 times the height of $\lambda e = 67.391$ mm. These values were obtained by utilizing parametric sweep functionality inside the COMSOL software.

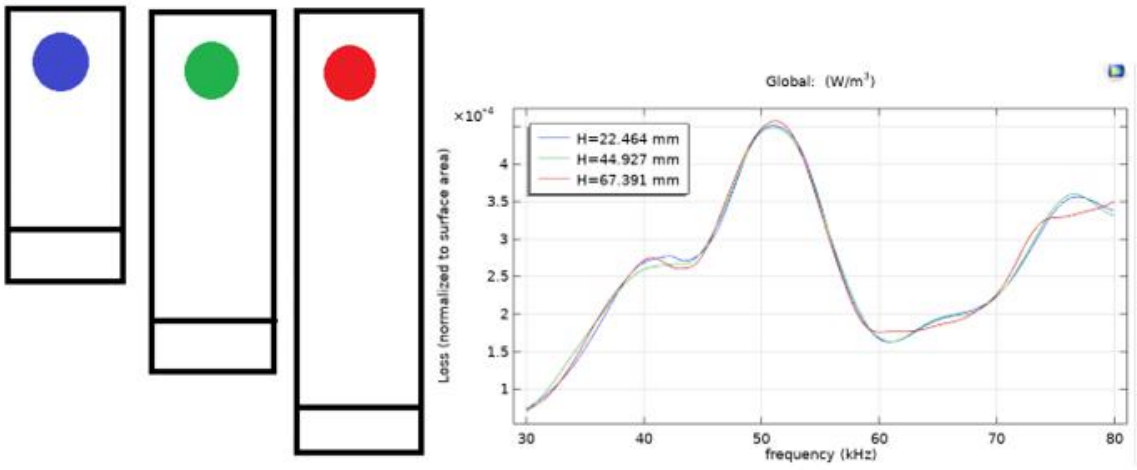

Figure 12(a) Changing the heights of the model (b) Loss vs frequency spectrum.

In Figure 12(a), the illustration illustrates a stationary sphere anchored at a specific point, while the measured distance from the bottom of the sphere gradually increases. Three separate diagrams portray distinct distances from the bottom of the sphere. Following a comprehensive exploration of these varying distances using the COMSOL simulation tool, we obtained a frequency spectrum, visually represented in Figure 12(b). Within this figure, the blue, green, and red diagrams correspond to the respective blue, green, and red spectra. Remarkably, the figure underscores a consistent resonance frequency of 51.0 kHz across all three spectra. This observation emphasizes the stability and constancy in the resonance behavior of the system, suggesting that alterations in the distances from the bottom of the sphere did not affect the resonance frequency.

Now, we aim to investigate the potential impact on our results when introducing two spheres positioned consecutively in Figure 13(a) and altering dimensions as illustrated in Figure 12(a). Following the simulation, an analysis of the loss versus frequency spectrum can be conducted, as depicted in Figure 13.

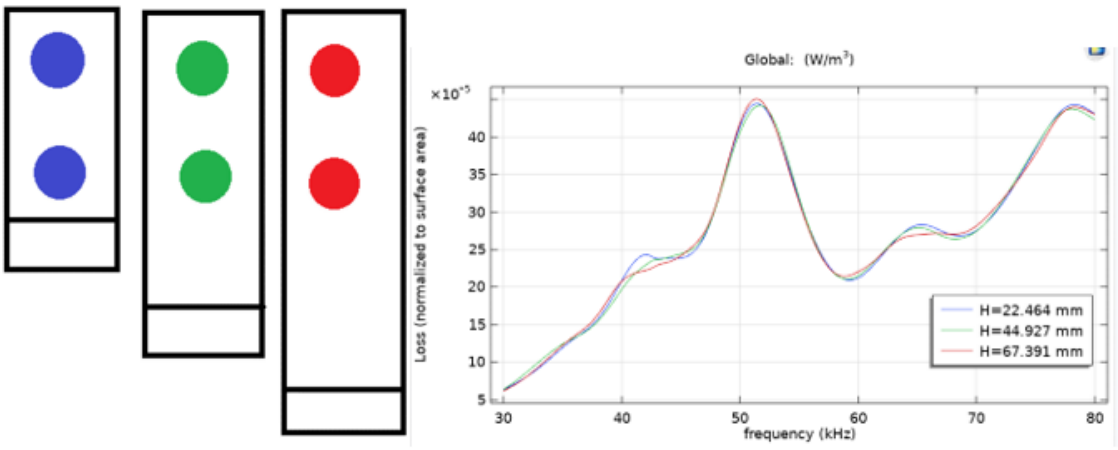

Figure 13(a) Changing the heights of the model with two spheres (b) Loss vs frequency spectrum.

Analyzing Figure 13 uncovers uniform blue, green, and red spectra among the spheres, with a slight shift in the resonance peak to 51.4 kHz compared to the resonance frequency of 51.0 kHz observed in the case of a single sphere. These findings currently offer compelling support for the stability of the model, emphasizing its negligible impact on our results.

Additional details regarding the stability of the model as influenced by alterations in the model's width can be in the Appendix.

4.4 Sweeping Sphere Radius

The objective at hand is to determine the absorption characteristics of tungsten loaded TPU by varying the sphere radii. The objective of our study is to analyze the distinct resonance peaks shown by tungsten loaded TPU spheres of varying radii. To accomplish this, we employed the parametric sweep technique in COMSOL to investigate various sphere radii ranging from 0.93 $\lambda_{TLR}/4$ to 1.14 $\lambda_{TLR}/4$ with an increment of 0.07 $\lambda_{TLR}/4$. The objective was to evaluate the resonant frequency response over a range of sphere sizes.

4.4.1 Loss vs. Frequency Spectrum

The presented spectrum Figure 14(b) illustrates the energy dissipation within the tungsten loaded TPU sphere at frequency intervals spanning from 30 kHz to 80 kHz. The loss within

the sphere was incorporated by integrating the entire surface of the sphere using COMSOL. Upon conducting the model simulation, we have obtained the loss versus frequency spectrum as follows:

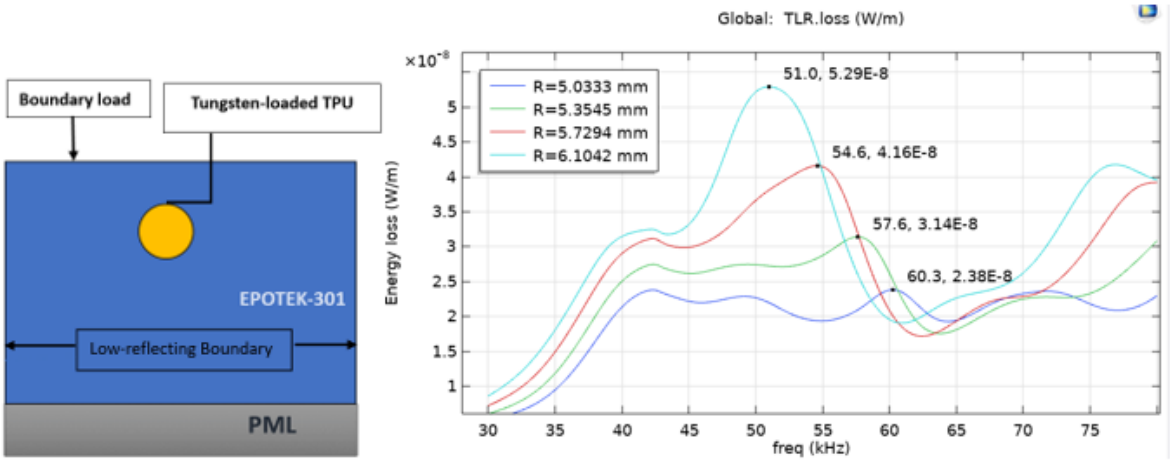

Figure 14(a) One sphere diagram (b) Loss vs. Frequency spectrum for sweeping different sizes of sphere.

Figure 14(b) displays four distinct resonant peaks, each corresponding to a different spherical size. The blue sphere is primarily characterized by a radius of 5.0 mm, which is equivalent to (0.93 $\lambda_{TLR}/4$). Additionally, it has a resonance frequency of 60.3 kHz. In the present context, the green spectrum corresponds to a sphere with a radius of 5.3 mm, calculated as ($\lambda_{TLR}/4$). This spectrum exhibits a resonant frequency of 57.6 kHz. On the other hand, the red spectrum corresponds to a sphere with a radius of 5.7 mm, calculated as (1.07 $\lambda_{TLR}/4$). This spectrum exhibits a resonant frequency of 54.6 kHz. The cyan spectrum is characterized by a radius of 6.1 mm, which corresponds to (1.14 $\lambda_{TLR}/4$). Additionally, the resonant frequency associated with this spectrum is 51.0 kHz. Within the overall spectrum, the cyan and red spectra stand out as particularly intriguing, primarily due to their distinctive feature of presenting a broad peak.

From our simulation results, it is evident that the resonance frequencies of spheres vary, and incrementally increasing the sphere mass results in corresponding decreases in resonance frequencies. For the largest sphere with a radius of 6.1 mm, the resonant frequency is observed at 51.0 kHz, while the smallest sphere with a radius of 5.0 mm exhibits a resonance frequency of 60 kHz. These variations show an inverse relationship with the mass of the

system, aligning with the principles of the mass-spring theory [35]. According to (Equation 16), the inverse relation between resonance frequency and mass is expressed as

$$\omega = \sqrt{\frac{k}{m}} \tag{16}$$

where ω represents the natural or resonance frequency, k is the stiffness constant, and m is the mass of the system. Our simulation results corroborate this theory, as an increase in mass, achieved by adding tungsten to the TPU, results in a lower resonant frequency.

4.4.2 Normalized Loss to Surface Area

To assess the efficacy of resonances accurately, it is crucial to mitigate the impact largely caused by an increased amount of dampening material. This phenomenon is referred to as normalized loss to surface area. The normalized loss to surface area can be obtained by dividing the energy loss by the surface area of the sphere. By doing a simulation similar to that described in Section 4.4.1, we may obtain the normalized loss to surface area vs. frequency spectrum as depicted below.

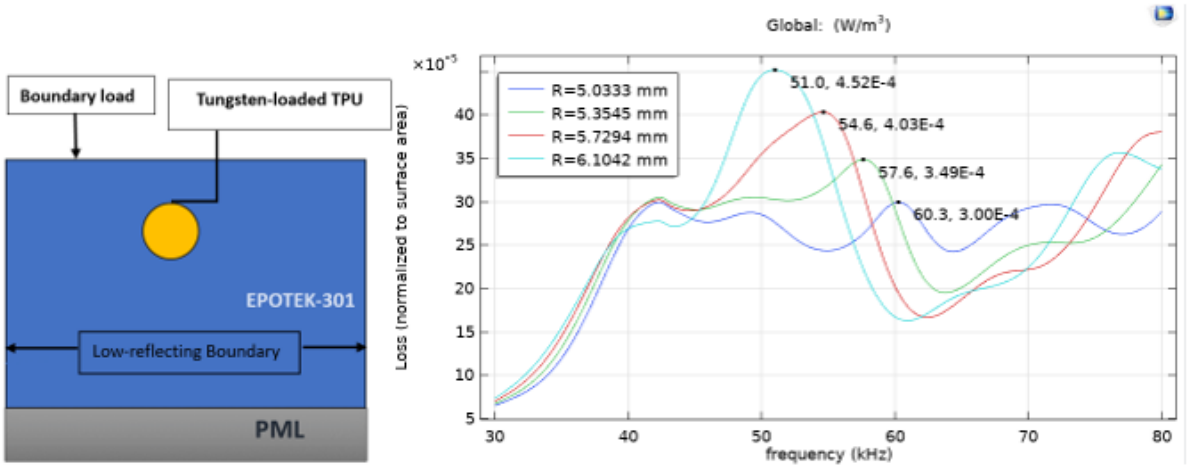

Figure 15(a) One sphere diagram (b) Normalized loss to the surface area vs. Frequency for sweeping different sizes of sphere.

In Figure 15(b), the resonant peaks seen are like those in Figure 14(b), only with strong varying amplitudes. This discrepancy in amplitude can be attributed to the influence of

dividing loss by the surface area. The specific frequency for a particular sphere can be determined by referring to the table provided.

Table 3 Specific resonant frequency for specific tungsten loaded TPU size

Radius of the sphere	Resonant frequency (kHz)
$(0.93\,\frac{\lambda_{TLR}}{4})$ or 5.0 mm	61
$(1.00\,\frac{\lambda_{TLR}}{4})$ or 5.3 mm	58
$(1.07\,\frac{\lambda_{TLR}}{4})$ or 5.7 mm	55
$(1.14\,\frac{\lambda_{TLR}}{4})$ or 6.1 mm	51

Analyzing Table 3 leads to a noteworthy conclusion regarding the fluctuations in resonance peaks corresponding to different sphere radii. It is evident that an approximate 7 to 8 percent increase in sphere size results in a corresponding 7 to 8 percent approximate decrease in resonance peaks. This correlation could prove valuable for individuals seeking a specific resonance frequency, as they can achieve it by adjusting sphere sizes in accordance with this mathematical relationship.

Figure 16 The correlation between resonant frequency and radius of the sphere. illustrates the relation between the resonant frequency and the radius of the sphere of single-sphere simulation.

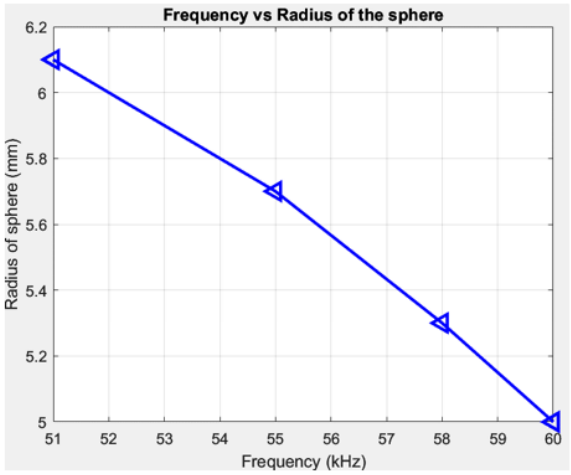

Figure 16 The correlation between resonant frequency and radius of the sphere.

4.5 Sweeping Radius of Two Spheres Maintaining a Fixed Spacing

In this section, we shall employ a pair of tungsten loaded TPU spheres for the purpose of energy absorption. To have a comprehensive understanding of the model, it is recommended to refer to Section 3.4. The proposed modification involves adjusting the radius of the spheres from 0.93 $\lambda_{TLR}/4$ to 1.14 $\lambda_{TLR}/4$. This will be done in increments of 0.07 $\lambda_{TLR}/4$ while keeping a distance of $\lambda e/4$ between the two spheres by using the parametric sweep method, as described in Section 3.4.3. The primary objective of this study is to investigate the impact of two spheres on the resonance frequency and compare it with that of a single sphere.

4.5.1 Normalized Loss to Surface Area

The following spectrum (Figure 17) reported in this study illustrates the normalized loss-to-surface area ratio across a frequency range of 30 kHz to 80 kHz for two consecutive spheres.

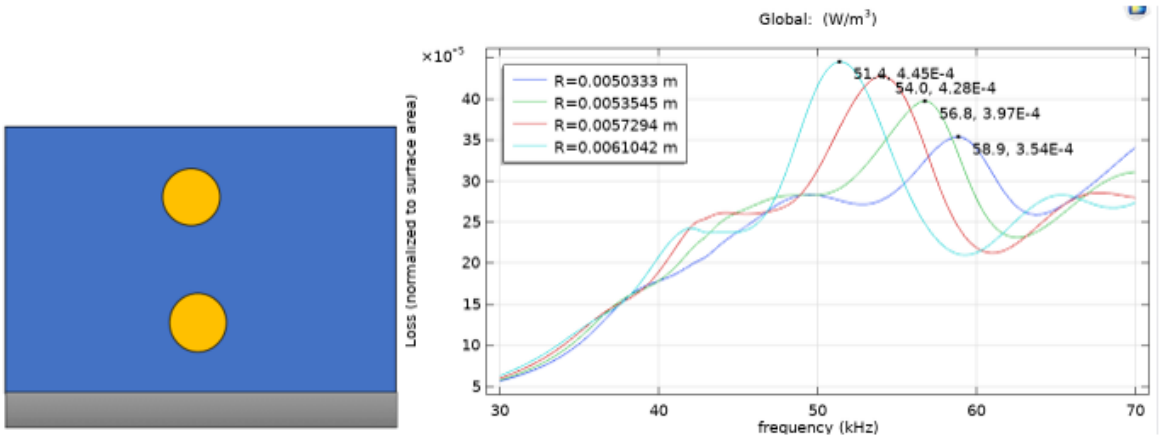

Figure 17(a) Two consecutive spheres diagram (b) Normalized loss to surface area vs frequency spectrum for two consecutive spheres.

In Figure 17 (b), the graph values correspond to the X and Y axes, where, for example, the blue spectrum represents 58.9 kHz on the X-axis and 3.54 X 10^{-4} Wm^{-3} on the Y-axis. This signifies that the frequency (X-axis) is 58.9 kHz, while the normalized loss to surface area (Y-axis) is 3.54 X 10^{-4} Wm^{-3}.

Upon comparing the spectra in Figure 15(b) and Figure 17(b), it becomes evident that the resonance frequency of the system of two identical spheres deviates from that of a single-sphere simulation. Observable variations and notable changes in amplitude occur due to wave interference effects and coupling effects between two spheres. The utilization of two spheres for absorption yields a higher absorption level compared to a single sphere. A closer examination of Y-axis values between single sphere Figure 15 (b) and double sphere Figure 17(b) simulations reveals varying losses. Consequently, the amplitude of the peaks fluctuates, exhibiting a pattern of increases and decreases when employing two identical spheres compared to a single sphere simulation, indicative of constructive and destructive interference between waves.

Examining Figure 17 (b) in contrast to Figure 15(b) reveals a noticeable shift in all resonance frequencies within the simulation involving two identical spheres compared to the single sphere simulation. This shift ranges approximately between 1 to 2 kHz, as outlined in Table 4. Particularly for the cyan spectrum, the resonance frequency shift is quite narrow, specifically at 0.4 kHz. Our analysis underscores that the use of identical spheres

significantly influences the modification of resonant frequencies and indeed exhibits a notable impact on altering the amplitude of the peaks when compared to the single-sphere simulation.

Table 4 Specific resonant frequency for specific tungsten-loaded TPU sphere.

Radius of the sphere	Resonant frequency (kHz) (two consecutive spheres simulation)	Resonant frequency (kHz) (single sphere simulation)
$(0.93 \frac{\lambda_{TLR}}{4})$ or 5.0 mm	59	61
$(1.00 \frac{\lambda_{TLR}}{4})$ or 5.3 mm	57	58
$(1.07 \frac{\lambda_{TLR}}{4})$ or 5.7 mm	54	55
$(1.14 \frac{\lambda_{TLR}}{4})$ or 6.1 mm	51	51

4.6 Sweeping Parametric Spacing between Two Spheres

In this study, we will examine the relationship between the separation of two spheres and its effect on altering the resonance frequency. Two spheres of equal size, defined as ($\lambda_{TLR}/4$), will be utilized in this study. The distance between the spheres will be varied incrementally, ranging from 1.43 λe/4 to 2.00 λe/4 with an increment of 0.19 λe/4. Upon doing this simulation, we will gain insights into the influence of the distance between two spheres on the alteration of the resonant frequency.

4.6.1 Normalized Loss to Surface Area

Upon the completion of the simulation, the resulting normalized loss to surface area against the frequency spectrum is as follows:

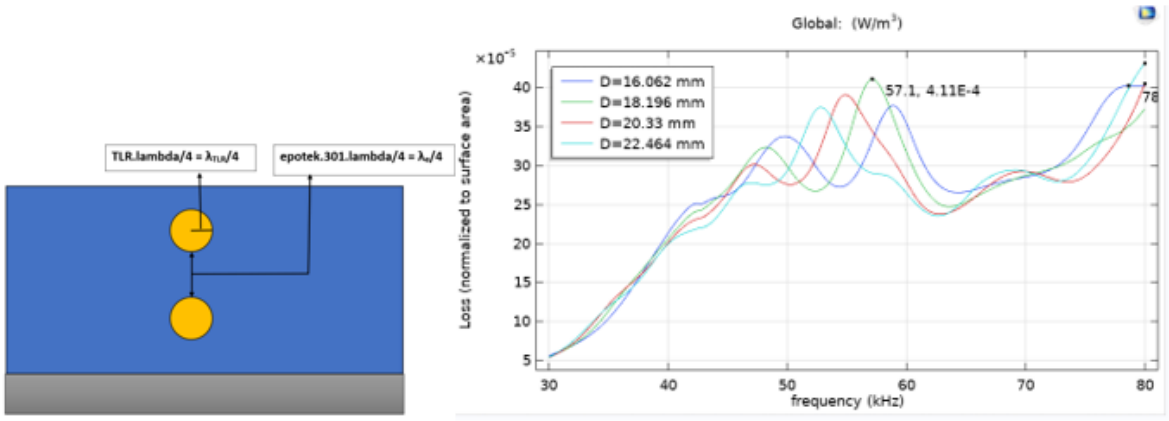

Figure 18(a) changes the spacing between two consecutive spheres.

(b)Normalized loss to surface area vs frequency spectrum for spacing between two spheres.

Figure 18(b) illustrates a graph featuring four distinct resonant peaks, each corresponding to varying distances between two tungsten loaded TPU spheres. These four distinct resonant peaks occur at frequencies of 58.9 kHz (depicted in blue), 57.1 kHz (in green), 54.9 kHz (in red), and 52.9 kHz (in cyan), while the distances between the two spheres are maintained at approximately 22 mm, 20 mm, 18 mm, and 16 mm, respectively.

It is evident that alterations in the spacing between consecutive spheres exert a significant influence on the resonant frequency. This influence follows an inverse relationship: as the distance between the spheres decreases, the resonant frequency increases because of the enhanced coupling effect. The coupling effect signifies a phenomenon where the oscillation of one sphere significantly influences the other. As the distance between two spheres decreases, the coupling effect intensifies, resulting in a collective higher resonance frequency and a shift towards higher values [36]. In our analysis, as depicted in Figure 18, a distinct correlation between the distances separating two spheres and the resonance frequency is evident. Specifically, an approximate 2 mm increase in distance corresponds to an approximately 2 kHz decrease in the resonant frequency, providing empirical support for the underlying theory. This is again a specific correlation between the resonant frequency and distance between two spheres. This precise correlation could prove valuable for individuals seeking a specific resonance frequency, as they can achieve it by adjusting the distance between these spheres in accordance with this mathematical relationship.

4.7 The Simulation between Two Different Sphere Sizes

Our current endeavor seeks to advance our exploration by expanding the bandwidth and achieving a broader peak within a specific resonance frequency. To accomplish this goal, we plan to conduct simulations involving two spheres with different radii.

In reference to Table 3, it becomes evident how the specific dimensions of a sphere can exert a pronounced influence on a corresponding resonant frequency. Each unique sphere size corresponds to a distinct resonant frequency. Until now, our simulations have involved the use of two spheres of identical size. However, our current objective is to introduce a new approach by utilizing two different sizes of tungsten loaded TPU spheres within a single simulation. The rationale for incorporating two distinct sphere sizes lies in our aim to create bandwidth. We are interested in observing the impact on the frequency spectrum when combining a sphere with a resonant frequency of 55 kHz and another sphere with a resonant frequency of 61 kHz. This amalgamation is anticipated to yield a bandwidth encompassing a specific frequency range lying between these two frequencies.

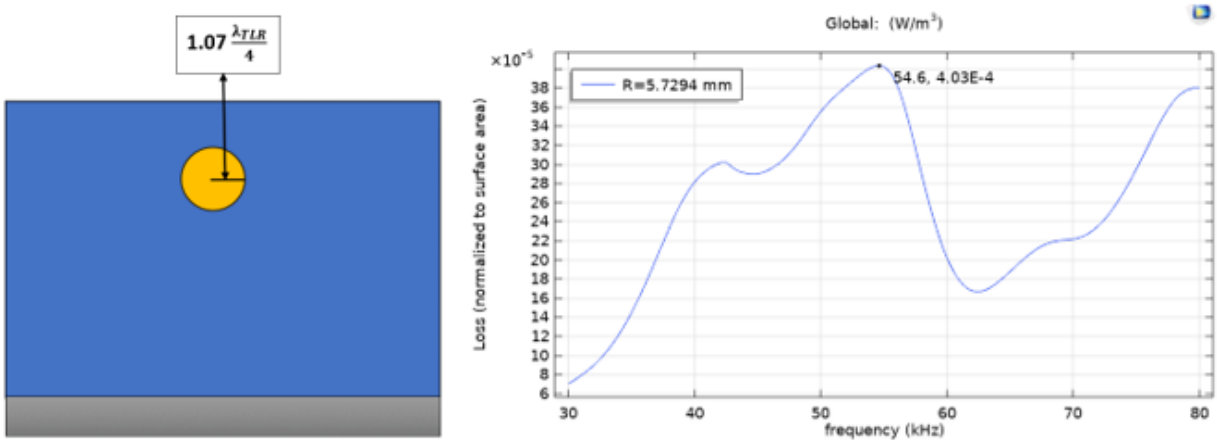

Figure 19(a) single sphere radius of 1.07 $\lambda_{TLR}/4$ (b) Loss vs frequency spectrum

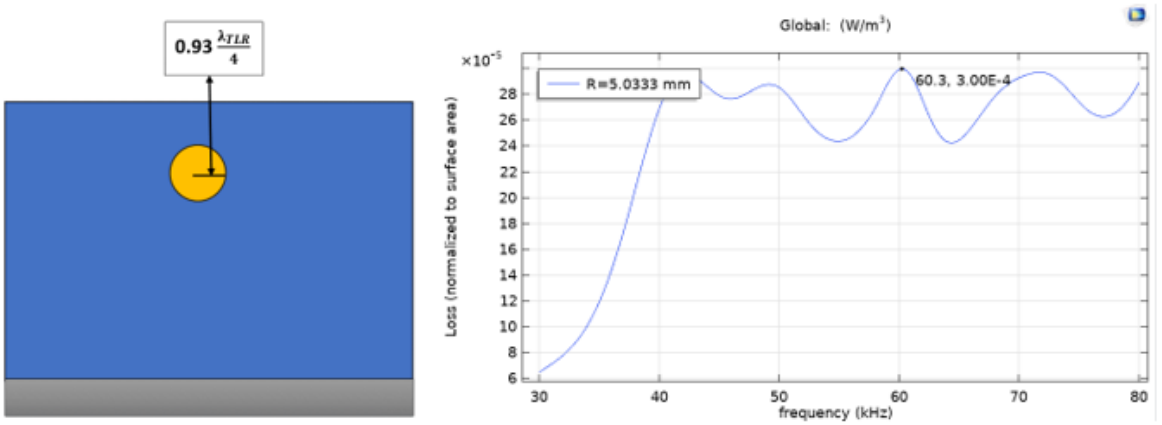

Figure 20(a) single sphere radius of 0.93 $\lambda_{TLR}/4$ *(b) Loss vs frequency spectrum*

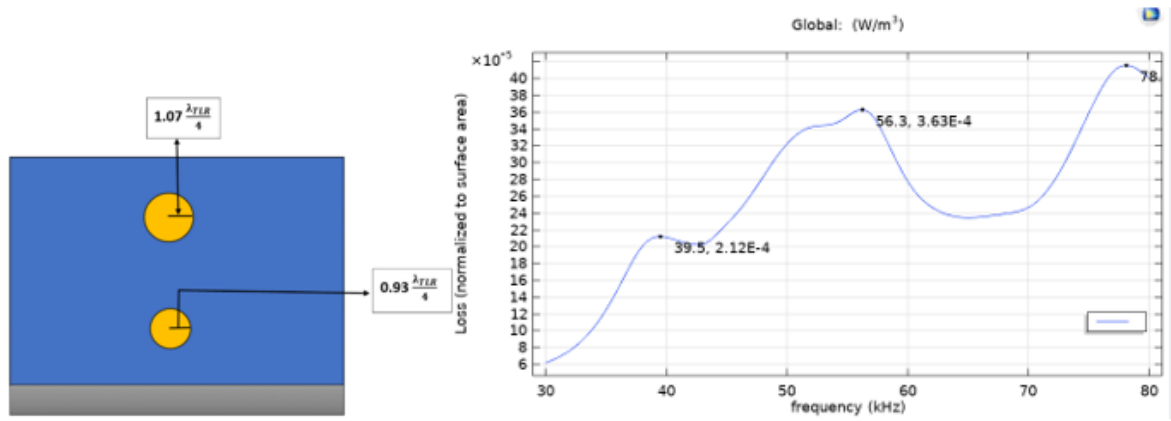

Figure 21 (a) combining of two different spheres radii of 1.07 $\lambda_{TLR}/4$ *and 0.93* $\lambda_{TLR}/4$ *respectively.*

(b) Simulation of two spheres of resonant frequency with 55 kHz and 61 kHz respectively.

Within Figure 21(b), we observe that the utilization of two distinct spheres, each possessing its own unique resonant frequency, results in the emergence of a specific frequency lying between these two distinct resonant frequencies. Notably, the resonant peak in this instance registers at 56.3 kHz, effectively positioning it between the two originally selected resonant frequencies of 55 kHz and 61 kHz and the bandwidth or peak at 56.3 kHz is observably

broader than what was observed in both the single-sphere simulation and the simulation involving two identical spheres.

For our subsequent exploration, we intend to repeat this process with another pair of two different spheres, wherein one sphere will have a resonant frequency of 51 kHz and the other will exhibit a frequency of 58 kHz.

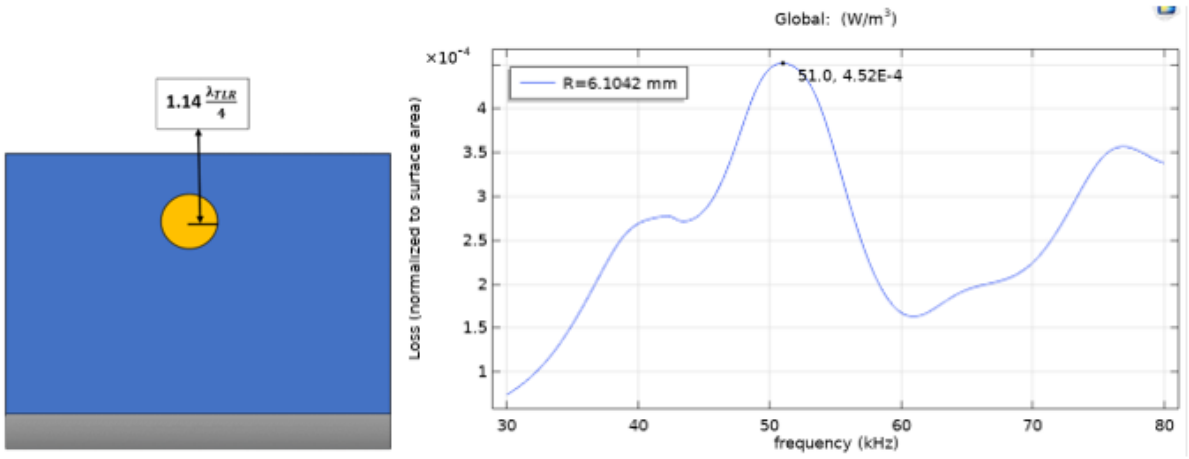

Figure 22(a) single sphere radius of 1.14 $\lambda_{TLR}/4$ (b) Loss vs frequency spectrum

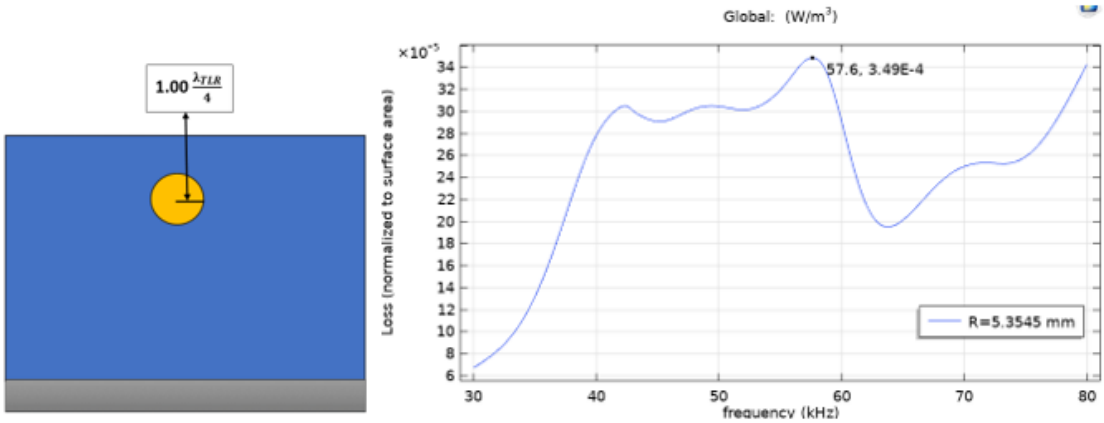

Figure 23(a) single sphere radius of 1.00 $\lambda_{TLR}/4$ (b) Loss vs frequency spectrum

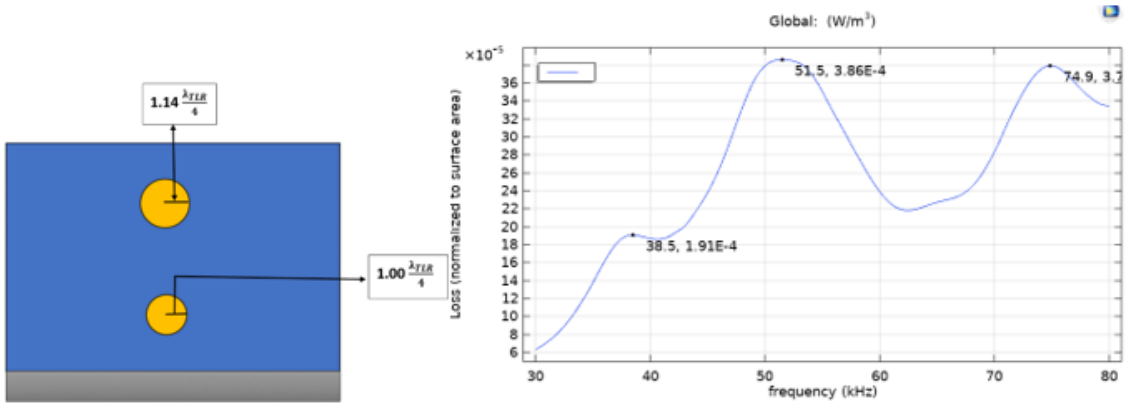

Figure 24 (a) combining of two different spheres radii of 1.14 $\lambda_{TLR}/4$ *and 1.00* $\lambda_{TLR}/4$ *respectively. (b) Simulation of two spheres of resonant frequency with 51 kHz and 58 kHz respectively.*

Based on the findings presented in Figure 24(b), where the resonant peak is measured at 51.5 kHz, falling within the range of 51 kHz and 58 kHz, it is evident that our initial assumption is confirmed. This illustrates that the choice of two distinct spheres can efficiently generate a broader peak or bandwidth compared to both the simulation involving single-sphere and the simulation involving two identical spheres. This phenomenon takes place when considering two different resonant frequencies, indicating dissimilar sphere sizes. It presents a practical approach to accomplishing our objective.

4.8 Effect of Spacing for Increasing Bandwidth or Broader Peak

In light of the observed impact on bandwidth resulting from the use of two different spheres, it is essential to acknowledge that altering the distance between the two spheres can also influence an increase in bandwidth or the creation of a broader peak. To shed light on this, our investigation involved varying the distance between two spheres across specific intervals: 0.75 λe/4 ,0.35 λe/4 and 0.05 λe/4. These variations were explored using two distinct spheres with resonant frequencies of 55 kHz and 61 kHz, corresponding to radii of 1.07 $\lambda_{TLR}/4$ and 0.93 $\lambda_{TLR}/4$, respectively. This comprehensive examination aims to elucidate the intricate relationship between sphere distance, resonance frequencies, and the resulting bandwidth characteristics.

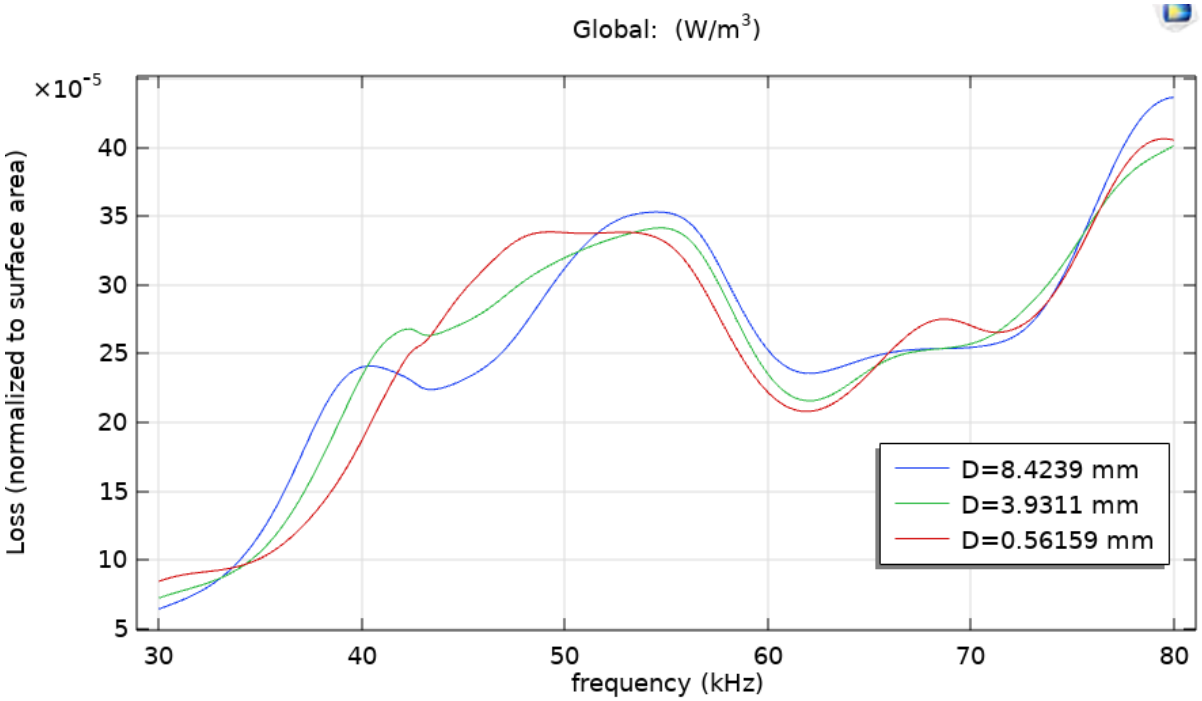

Figure 25 Changing the distance between two different spheres.

In Figure 25, it becomes visible that transitioning between two distinct spheres plays a crucial role in augmenting bandwidth. Notably, as the distance between the two different spheres decreases, there is a corresponding increase in bandwidth attributed to the coupling effect between them. Upon concluding the experiment, it becomes apparent that employing two different spheres and adjusting the distance between them significantly impacts the enhancement of bandwidth.

5 Discussion

The findings of our investigation relating to the acoustic properties within the metamaterial, specifically the computational modeling of tungsten loaded TPU and epoxy (Epotek 301-2), provide significant knowledge regarding the resonance attributes and energy dissipation of the composite structures. Nevertheless, it is imperative to undertake a thorough analysis of the uncertainties, limitations, and unanticipated discoveries inside our methodology.

5.1 Discussion about Findings and Their Necessities

Our research has unveiled a distinct relationship between sphere radius and resonance frequency (Section 4.4.2). Furthermore, we've established a mathematical relationship between the distance separating consecutive spheres and resonance frequency (Section 4.6.1). Translating these findings into the manufacturing of tangible tungsten loaded TPU samples necessitates addressing answers to some crucial questions:

Achieving a Flat Absorption Coefficient across the Desired Bandwidth:

The critical aspect of achieving a flat absorption coefficient across the desired bandwidth is evident in Figure 25. The spacing between two distinct spheres plays a pivotal role. Notably, reducing the gap gradually enhances flat absorption. Analyzing Figure 25, a decrease in spacing from around 8 mm to 4 mm results in a flatter absorption (green) compared to the blue spectrum. Further reduction, from 4 mm to 0.5 mm, enhances the flatness, as indicated by the red spectrum. In essence, decreasing the spacing between spheres, as illustrated, is key to achieving a more uniformly flat absorption across the desired bandwidth.

Scaling the Absorption Coefficient:

The absorption coefficient can be scaled by employing diverse strategies. Comparing Figure 15(b) and Figure 17(b), it is obvious that using two consecutive spheres, as opposed to a single sphere, alters the absorption coefficient. Additionally, adjusting the concentration of tungsten within the TPU also allows precise control. Increasing tungsten concentration elevates the overall mass, contributing to improved absorption. However, careful consideration must be given to bulk modulus and Poisson ratio, as the latter introduces uncertainties in absolute dimensions owing to tungsten's unique properties.

Feasibility of Additive Manufacturing:

Several factors impact the feasibility of manufacturing tungsten loaded rubber, including the choice of an additive manufacturing technique. Essential criteria include high precision, resolution, and robust adhesion between materials, particularly between tungsten and TPU.

After thorough analysis, the Selective Laser Sintering (SLS) technique emerged as the most suitable among various additive manufacturing methods. The decision is rooted in SLS's ability which has been discussed in the next section.

In summary, our exploration of the relationship between sphere characteristics and resonance frequency serves as a foundation for addressing practical manufacturing considerations. Answering these questions not only advances our understanding of metamaterial behavior but also guides the practical realization of tungsten loaded TPU metamaterials for real-world applications.

5.2 Discussion of Best Technique to Manufacture Tungsten Loaded TPU

Each additive manufacturing technology possesses distinct advantages and disadvantages when employed for the production of various metamaterials [6]. In our study on the metamaterial tungsten loaded TPU, we have determined that Selective Laser Sintering (SLS) stands out as the most optimal additive manufacturing technology. This selection is based on the notable advantages it offers. Selective Laser Sintering (SLS) is a manufacturing technique that offers the utilization of a diverse array of materials, such as polymers (Nylon, TPU, Polyetherimide, etc.), metal powders (Aluminum, Titanium, Stainless Steels, etc), ceramics (Alumina, Zirconia, etc.) [37]. Notably, SLS exhibits exceptional precision, and resolution and the laser spot size in SLS printers ranges from 50 to 200 micrometers [37], depending on the printer model and settings, facilitating the creation of intricate three-dimensional structures using a layer-by-layer approach. Industrial SLS printers can offer build volumes of up to 1000 x 1000 x 1000 millimeters or larger [37]. Furthermore, this method ensures robust adhesion between layers [38], resulting in the fabrication of highly durable objects. Simultaneous production of several components is also achievable with the utilization of SLS. The numerous benefits associated with the SLS method have provided us with an opportunity to consider this technology as a viable option for the production of tungsten loaded TPU. However, it is important to acknowledge that SLS does generate a certain amount of waste [38].

Conversely, alternative methodologies possess some drawbacks that are deemed highly undesirable in the production of our metamaterial. Fused Deposition Modelling (FDM) encounters challenges in achieving high precision and requires meticulous attention to detail in order to fabricate intricate metamaterial structures. On the other hand, Electron Beam Melting (EBM) has mostly been employed for metal powders rather than polymers, hence posing issues in selecting an appropriate manufacturing method for our desired metamaterial. Both Stereolithography (SLA) and inkjet 3D printing encounter obstacles in achieving high resolution and desired composition.

5.3 Relation between Theory and Expected Result

The analytical and logical explanation of the resonance frequency of a sphere in our simulation results can be attributed to numerous crucial variables.

5.3.1 Mass-Spring System

The simulation we have developed adheres to the fundamental principles of a mass-spring system. Based on the principles of the mass-spring theory, as described by Equation 4.1, it can be observed that the resonance frequency (ω) exhibits an inverse relationship with the square root of the mass (m). The essential connection highlighted in this context emphasizes the significant influence of mass in defining the inherent frequency of the system.

In our work, the inclusion of tungsten in the TPU spheres results in an increase in mass inside the system. The mass of the sphere grows proportionally to the increase in its radius, leading to a corresponding decrease in the resonance frequency. The observed inverse relationship is consistent with our simulation results.

5.3.2 Effect of Material Properties

The selection of materials, such as tungsten loaded TPU, induces alterations in the stiffness of the system. The total dynamics are influenced by the interaction between the mass derived from tungsten and the stiffness of the material. Examining the distinct characteristics of the material properties and their influence on the response of the system can yield a further

understanding of the reported resonance frequencies. This incorporates the factors of Young's modulus, density, and Poisson's ratio.

5.3.3 Coupling Effects and Damping

The resonance frequency is significantly influenced by the coupling effects and damping present inside the material. The simulation reveals that the resonance behaviors are governed by the interaction between the spheres. The coupling and damping mechanisms (Section 4.6.1) within the system explain the processes by which energy is transported and dissipated, in addition to explaining the presence of resonance peaks.

In brief, the resonance frequency exhibited by a particular sphere within our simulation findings can be related to a convergence of factors including the mass-spring model, material characteristics, and coupling phenomena. The detailed examination of these factors offers a rational and thorough justification for the observed peaks in our frequency spectrum.

5.4 Possible Uncertainties and Weaknesses of Our Proposed Model

The present study offers significant contributions to the understanding of interaction effects in the acoustic behavior of metamaterial spheres. However, it is crucial to note the presence of uncertainties and limitations in our methodology. The analytical calculations may be subject to uncertainty due to the assumptions made on Poisson's ratio and bulk modulus of tungsten loaded TPU. Moreover, it should be noted that the simulation model's dependence on certain material features and boundary conditions may not comprehensively encompass the complex dynamics of acoustic interactions in the real world. The simplifications employed in our model, such as assuming uniform material properties and idealized boundary conditions, may introduce certain restrictions that could affect the accuracy of our findings.

5.5 Unexpected Findings

We noticed something surprising – the calculated speed of sound and the simulated speed of sound for tungsten loaded TPU and epoxy material Epotek 301-2 are very close. Even though our calculations are based on certain assumptions, the simulation results match well with our

calculations. This unexpected agreement raises questions about the reliability of our assumptions and highlights the need for further investigation into the specific factors causing this alignment.

5.6 Relation Between Our Results to The Other Studies

In our investigation, we delved into the mass-spring theory to ascertain the resonance frequency of a specific sphere within the proposed metamaterial known as tungsten loaded TPU. Our findings revealed an inverse relationship between the mass or radius of the sphere and the resonance frequency of the system. Increasing the system's mass is achieved by enlarging the sphere's radius, leading to a corresponding decrease in the resonance frequency.

Drawing parallels to Li Min et al.'s [39] exploration of a conventional metamaterial structure, the rectangular metallic antenna, we observed resonance mechanisms in the metamaterial. Li Min identified the resonance wavelength ($\lambda 0$) as varying with the size of the metamaterial unit structure, specifically the length of the antenna (l). A proportional relationship was maintained, indicating that an increase in the antenna's length resulted in a corresponding increase in the resonance wavelength. Given the inverse relationship between wavelength and frequency, we deduced that the resonance frequency is inversely proportional to the size of the antenna, represented by the length of the antenna.

Xiaoming Liu et al. [40] focused on a Mie resonance-based metamaterial perfect absorber (MPA) composed of a dielectric cube and copper. Their observations indicated that the absorption peak of the Mie resonance based MPA changes with variations in the size of the dielectric cube. The study demonstrated a clear inverse relationship, as the simulated absorption peak frequency decreased from 11.09 GHz to 9.02 GHz with an increase in the side length (a) of the dielectric cube from 1.9 mm to 2.1 mm.

Son Tung Bui et al. [41] proposed a small-sized metamaterial perfect absorber with a sandglass structure. Their investigation highlighted the strong influence of the geometrical parameter (l), representing the length of the zigzag wire in the sandglass structure, on the absorption frequency. A notable inverse relationship was observed, as the absorption frequency significantly decreased from 452 to 323 MHz when the parameter l was increased from 1 to 5 mm.

P.V. Tuong et al. [42] introduced a perfect-absorber metamaterial based on a flower-shaped structure. Through meticulous investigation, it was established that the frequency of the perfect absorber peak is governed by the size of the flower (radius r). A quantitative relationship emerged, revealing an inverse proportionality of the resonance frequency with the square root of the radius.

In a similar vein, Nishant et al. [43] proposed a LiTaO3-based metamaterial perfect absorber for the terahertz spectrum. The resonant wavelength of the metamaterial was found to be proportional to the radius of the metamaterial, and an empirical formula was established to express the resonant wavelength as a function of the radius.

The exploration of the coupling effect emerged as a pivotal theory in our thesis, explaining the dynamic interaction between two spheres and their resonance frequencies. Our research underscores a noteworthy observation: as the proximity between the two spheres decreases, the coupling effects intensify. This heightened coupling effect significantly influences the resonance frequency. Notably, our investigation reveals a direct correlation—the closer the spheres, the stronger the coupling effect, leading to an elevated resonance frequency. Thus, our findings establish a proportional relationship between coupling effects and resonance frequency in the context of our study.

In their article, Gao et al. [44] illustrated the coupling effect in dielectric metamaterials through a meticulous examination of adjacent resonator distances. The study delves into the impact of the separation between two dielectric cubes on coupling phenomena. Gao investigated the changes in magnetic resonance frequency within the structure when the distance between two dielectric cubes was varied, ranging from 0.5 μm to 2 μm. The findings revealed a discernible trend: as the distance of the dielectric cube along the electric field direction increased, the magnetic resonance frequency decreased from 7 THz to 5 THz.

6 Conclusion

The objective of this study is to investigate the development of backing materials for low-frequency underwater acoustic transducers using tungsten loaded TPU scaffolds. The study specifically focuses on examining the effects of resonance frequency, bandwidth, and efficiency. This study investigates the effects of numerous parameters, such as sphere size, spacing, and combinations of resonant frequencies, on the acoustic characteristics and efficacy of the metamaterial. The finite element approach (COMSOL simulation) is employed to analyze and evaluate these impacts. The results reported in this study provide useful insights into the possible applications and benefits of utilizing constructed metamaterials to enhance the performance of underwater acoustic transducers.

The conducted simulations have provided a detailed understanding of the acoustic behavior of tungsten loaded TPU scaffolds. The analysis of single and consecutive sphere simulations demonstrated a distinct association between the size of the sphere and its resonance frequency. The parametric sweep of sphere radii effectively confirmed the predicted inverse relationship between mass and resonant frequency, as postulated by the mass-spring theory. This relationship yields a significant conclusion concerning the variations in resonance peaks associated with distinct sphere radii. The data clearly indicates that a change in sphere size of approximately 7 to 8 percent leads to a corresponding approximate decrease of 7 to 8 percent in resonance peaks. The precise connection shown above holds potential value for those who are looking to attain a specific resonance frequency. By altering the sizes of the spheres in accordance with this mathematical relationship, they can effectively reach their desired resonance frequency.

Moreover, the examination of the influence of the spatial separation between two spherical objects underscored the importance of distance in modifying the resonance frequencies. The empirical correlation between the distance between spheres and the resonant frequency, which is attributed to the coupling phenomenon, offers a pragmatic comprehension of how the distance parameter can be modified to attain desired resonance frequencies. This relationship yields a significant conclusion concerning the variations in resonance peaks

associated with the distance between two consecutive spheres. The data clearly indicates that an increase in distance between two consecutive spheres by approximately 2mm leads to a corresponding approximate decrease of 2 kHz in resonance peaks. Again, this precise connection shown above holds potential value for those who are looking to attain a specific resonance frequency.

The introduction of two spheres with different sizes successfully demonstrated the generation of broader bandwidths compared to single-sphere and identical-sphere simulations. This outcome signifies a potential avenue for optimizing underwater acoustic transducer designs by carefully selecting sphere sizes and adjusting their spacing.

In summary, this study makes a valuable contribution to the field of underwater acoustics through its comprehensive investigation of the acoustic properties shown by tungsten loaded TPU scaffolds. The empirical associations observed between different variables and their influence on resonance frequencies establish a fundamental basis for the development of metamaterials customized to meet certain frequency criteria. The research presented in this study has the potential to be applied in various ways, particularly in the improvement of low-frequency underwater acoustic transducers. It provides a comprehensive understanding of how engineered materials can be effectively utilized to attain specific performance characteristics. The results of this study can provide valuable insights for future research in the field of underwater acoustic transducers, specifically in the advancement of specialized backing materials. The acquisition of knowledge through quantitative analysis of acoustic behavior and the examination of various parameters can provide valuable insights for design purposes. This can ultimately result in the development of customized metamaterials that are tailored for specific frequency ranges. Furthermore, some potential areas for further research have been discussed in the following section.

7 Suggestions for Future Research and Development

Upon concluding this investigation, we have identified some promising directions for future research and development stemming from this thesis. In our study, we made certain assumptions about the material properties of tungsten loaded TPU, which, while providing

valuable insights, did not yield precise results for manufacturing the desired metamaterial. To advance our work, the following areas warrant further exploration:

Optimizing Metamaterial Design: As we look ahead, a promising area for further study involves using theoretical models to design filters in metamaterials. We can explore how combining resonating structures can create special configurations like band-stop or band-pass filters. This approach offers great potential for improving metamaterial performance in different applications. By using theoretical frameworks, we aim to have better control over the way sound behaves. This future research can help us fine-tune the composition and structure of metamaterials, making them work better for various needs. Ultimately, it's about creating more versatile and effective designs.

Manufacturing of Real Tungsten Loaded TPU:

Since we made assumptions about the majority of the material properties for tungsten loaded TPU, it is imperative to physically manufacture it to ascertain the actual properties resulting from the amalgamation of tungsten with TPU. Obtaining these real values is crucial for gaining a more accurate understanding of our investigation.

As part of future work for the thesis, it is recommended to further investigate the interconnects between the spheres in the context of tungsten loaded TPU manufacturing. Consideration should be given to exploring the necessity and implications of incorporating "rods" or other structural elements between the spheres. This inquiry becomes particularly relevant if the intention is to construct a scaffold to support the spheres before encapsulation. Examining the role and design of such interconnects would provide valuable insights into optimizing the structural integrity of the system under consideration.

References

[1] I. F. Akyildiz, D. Pompili, and T. Melodia, “Underwater acoustic sensor networks: research challenges,” Ad Hoc Netw., vol. 3, no. 3, pp. 257–279, May 2005, doi: 10.1016/j.adhoc.2005.01.004.

[2] L. Shams and T.-B. Xu, “Underwater communication acoustic transducers: a technology review,” in Sensors and Smart Structures Technologies for Civil, Mechanical, and Aerospace Systems 2023, Z. Su, M. P. Limongelli, and B. Glisic, Eds., Long Beach, United States: SPIE, Apr. 2023, p. 8. doi: 10.1117/12.2663073.

[3] M. R. Haberman and M. D. Guild, “Acoustic metamaterials,” Phys. Today, vol. 69, no. 6, pp. 42–48, Jun. 2016, doi: 10.1063/PT.3.3198.

[4] M. Yang and P. Sheng, “Sound Absorption Structures: From Porous Media to Acoustic Metamaterials,” Annu. Rev. Mater. Res., vol. 47, no. 1, pp. 83–114, 2017, doi: 10.1146/annurev-matsci-070616-124032.

[5] “Acoustic metamaterials: From local resonances to broad horizons.” Accessed: Aug. 17, 2023. [Online]. Available: https://www.science.org/doi/10.1126/sciadv.1501595

[6] M. Askari et al., “Additive manufacturing of metamaterials: A review,” Addit. Manuf., vol. 36, p. 101562, Dec. 2020, doi: 10.1016/j.addma.2020.101562.

[7] K. K. Shung and M. Zippuro, “Ultrasonic transducers and arrays,” IEEE Eng. Med. Biol. Mag., vol. 15, no. 6, pp. 20–30, Dec. 1996, doi: 10.1109/51.544509.

[8] S. S. Rojas, S. Tridandapani, and B. D. Lindsey, “A thin, high penetration depth phased array transducer with a metamaterial acoustic backing for cardiac imaging with X-ray computed tomography compatibility,” in 2021 IEEE International Ultrasonics Symposium (IUS), Xi’an, China: IEEE, Sep. 2021, pp. 1–4. doi: 10.1109/IUS52206.2021.9593512.

[9] V. M. Do Nascimento, V. L. D. S. Nantes Button, J. M. Maia, E. T. Costa, and E. J. V. Oliveira, “Influence of backing and matching layers in ultrasound transducer

performance," presented at the Medical Imaging 2003, W. F. Walker and M. F. Insana, Eds., San Diego, CA, May 2003, p. 86. doi: 10.1117/12.479924.

[10] R. Feynman, Lectures in Physics, vol. Volume 1, Chapter 47. in Sound. The wave equation, vol. Volume 1, Chapter 47. [Online]. Available: https://www.feynmanlectures.caltech.edu/I_47.html

[11] "17-2-speed-of-sound." Accessed: Oct. 19, 2023. [Online]. Available: https://courses.lumenlearning.com/suny-osuniversityphysics/chapter/17-2-speed-of-sound/

[12] M. Aziman, Z. A. M. Hazreek, A. T. S. Azhar, and D. S. Haimi, "Compressive and Shear Wave Velocity Profiles using Seismic Refraction Technique," J. Phys. Conf. Ser., vol. 710, p. 012011, Apr. 2016, doi: 10.1088/1742-6596/710/1/012011.

[13] "Compressional Wave - an overview | ScienceDirect Topics." Accessed: Nov. 07, 2023. [Online]. Available: https://www-sciencedirect-com.ezproxy1.usn.no/topics/engineering/compressional-wave

[14] Lurton, Xavier, An Introduction to Underwater Acoustics—Principles and Applications, 2nd ed. [Online]. Available: https://books.google.no/books?hl=en&lr=&id=VTNRh3pyCyMC&oi=fnd&pg=PR11&dq=acoustic+attenuation+for+underwater+acoustic+transducer&ots=m-CuxEPOwL&sig=AmqbReseFvGbdfzXC_6tNNsa9z8&redir_esc=y#v=onepage&q=acoustic%20attenuation%20for%20underwater%20acoustic%20transducer&f=false

[15] T. Cambonie, F. Mbailassem, and E. Gourdon, "Bending a quarter wavelength resonator : Curvature effects on sound absorption properties," Appl. Acoust., vol. 131, pp. 87–102, Feb. 2018, doi: 10.1016/j.apacoust.2017.10.004.

[16] C. H. Sohn and J. H. Park, "A comparative study on acoustic damping induced by half-wave, quarter-wave, and Helmholtz resonators," Aerosp. Sci. Technol., vol. 15, no. 8, pp. 606–614, Dec. 2011, doi: 10.1016/j.ast.2010.12.004.

[17] G. Catapane, G. Petrone, O. Robin, and K. Verdière, "Coiled quarter wavelength resonators for low-frequency sound absorption under plane wave and diffuse acoustic field

excitations," Appl. Acoust., vol. 209, p. 109402, Jun. 2023, doi: 10.1016/j.apacoust.2023.109402.

[18] "destructive-interference." Accessed: Sep. 28, 2023. [Online]. Available: https://byjus.com/physics/destructive-interference/

[19] K. Anas, S. David, R. R. Babu, M. Selvakumar, and S. Chattopadhyay, "Energy dissipation characteristics of crosslinks in natural rubber: an assessment using low and high-frequency analyzer," J. Polym. Eng., vol. 38, no. 8, pp. 723–729, Aug. 2018, doi: 10.1515/polyeng-2016-0425.

[20] X. Zeng, "NBR/CR-Based High-Damping Rubber Composites Containing Multiscale Structures for Tailoring Sound Insulation", doi: https://doi.org/10.1002/mame.202200464.

[21] B. Chen, J. Dai, T. Song, and Q. Guan, "Research and Development of High-Performance High-Damping Rubber Materials for High-Damping Rubber Isolation Bearings: A Review," Polymers, vol. 14, no. 12, p. 2427, Jun. 2022, doi: 10.3390/polym14122427.

[22] D. Hidayat, N. S. Syafei, B. M. Wibawa, M. Taufik, A. Bahtiar, and Risdiana, "Metal-Polymer Composite as an Acoustic Attenuating Material for Ultrasonic Transducers," Key Eng. Mater., vol. 860, pp. 303–309, Aug. 2020, doi: 10.4028/www.scientific.net/KEM.860.303.

[23] T. Stephen T. and B. M. Jerry, Classical Dynamics of Particles and Systems, 5th ed. California. [Online]. Available: https://faculty.washington.edu/seattle/physics227/reading/reading-2b.pdf

[24] "tungsten-w." Accessed: Oct. 25, 2023. [Online]. Available: https://www.tungsten.com/material-info/tungsten-w

[25] D. Tabor, "The bulk modulus of rubber," Polymer, vol. 35, no. 13, pp. 2759–2763, Jun. 1994, doi: 10.1016/0032-3861(94)90304-2.

[26] C.-S. Man and M. Huang, "A Simple Explicit Formula for the Voigt-Reuss-Hill Average of Elastic Polycrystals with Arbitrary Crystal and Texture Symmetries," J. Elast., vol. 105, no. 1–2, pp. 29–48, Nov. 2011, doi: 10.1007/s10659-011-9312-y.

[27] E. E. Villalobos-Portillo, L. Fuentes-Montero, M. E. Montero-Cabrera, D. C. Burciaga-Valencia, and L. E. Fuentes-Cobas, “Polycrystal piezoelectricity: revisiting the Voigt-Reuss-Hill approximation,” Mater. Res. Express, vol. 6, no. 11, p. 115705, Oct. 2019, doi: 10.1088/2053-1591/ab46f2.

[28] “Isotropic loss factor.” Accessed: Nov. 28, 2023. [Online]. Available: https://doc.comsol.com/5.5/doc/com.comsol.help.sme/sme_ug_solid.07.30.html

[29] P. Foteinopoulos, P. Stavropoulos, A. Papacharalampopoulos, and G. Chryssolouris, “Unified Approach in Design and Manufacturing Optimization of Hybrid Metal-composites Parts,” Procedia CIRP, vol. 55, pp. 59–64, 2016, doi: 10.1016/j.procir.2016.09.035.

[30] Haifeng Wang, T. Ritter, Wenwu Cao, and K. K. Shung, “High frequency properties of passive materials for ultrasonic transducers,” IEEE Trans. Ultrason. Ferroelectr. Freq. Control, vol. 48, no. 1, pp. 78–84, Jan. 2001, doi: 10.1109/58.895911.

[31] “Isotropic loss factor.” Accessed: Nov. 26, 2023. [Online]. Available: https://www.comsol.com/blogs/damping-in-structural-dynamics-theory-and-sources/

[32] “Low Reflecting Boundary.” Accessed: Nov. 14, 2023. [Online]. Available: https://doc.comsol.com/5.5/doc/com.comsol.help.sme/sme_ug_solid.07.72.html

[33] “Nyquist Theorem.” Accessed: Nov. 11, 2023. [Online]. Available: https://www.comsol.com/blogs/simulation-tools-for-solving-wave-electromagnetics-problems/

[34] “performing-parametric-sweep-study-comsol-multiphysics.” Accessed: Oct. 04, 2023. [Online]. Available: https://www.comsol.com/video/performing-parametric-sweep-study-comsol-multiphysics

[35] R. Blickhan, “The spring-mass model for running and hopping,” J. Biomech., vol. 22, no. 11–12, pp. 1217–1227, Jan. 1989, doi: 10.1016/0021-9290(89)90224-8.

[36] G. Catapane, “Coupling effect of acoustic resonators for low-frequency sound suppression,” presented at the Aeronautics and Astronautics, Dec. 2023, pp. 254–257. doi: 10.21741/9781644902813-55.

[37] “sls2.” Accessed: Nov. 28, 2023. [Online]. Available: https://www.wevolver.com/article/sls-printing-unlocking-the-potential-of-selective-laser-sintering

[38] “SLS technique.” Accessed: Nov. 27, 2023. [Online]. Available: https://www.protolabs.com/en-gb/resources/blog/selective-laser-sintering-its-advantages-and-disadvantages/

[39] L. Min and L. Huang, “Perspective on resonances of metamaterials,” Opt. Express, vol. 23, no. 15, p. 19022, Jul. 2015, doi: 10.1364/OE.23.019022.

[40] X. Liu, Q. Zhao, C. Lan, and J. Zhou, “Isotropic Mie resonance-based metamaterial perfect absorber,” Appl. Phys. Lett., vol. 103, no. 3, p. 031910, Jul. 2013, doi: 10.1063/1.4813914.

[41] S. Tung Bui et al., “Small-size metamaterial perfect absorber operating at low frequency,” Adv. Nat. Sci. Nanosci. Nanotechnol., vol. 5, no. 4, p. 045008, Nov. 2014, doi: 10.1088/2043-6262/5/4/045008.

[42] P. V. Tuong, V. D. Lam, J. W. Park, E. H. Choi, S. A. Nikitov, and Y. P. Lee, “Perfect-absorber metamaterial based on flower-shaped structure,” Photonics Nanostructures - Fundam. Appl., vol. 11, no. 1, pp. 89–94, Feb. 2013, doi: 10.1016/j.photonics.2012.09.002.

[43] N. Shankhwar, Y. Kalra, and R. K. Sinha, “LiTaO3 based metamaterial perfect absorber for terahertz spectrum,” Superlattices Microstruct., vol. 111, pp. 754–759, Nov. 2017, doi: 10.1016/j.spmi.2017.07.034.

[44] J. Gao, Y. Zhang, Y. Sun, and Q. Wu, “Coupling effects in dielectric metamaterials,” Results Phys., vol. 17, p. 103038, Jun. 2020, doi: 10.1016/j.rinp.2020.103038.

List of tables and figures

Appendix